

Pseudo-irreversible butyrylcholinesterase inhibitors: SAR, kinetic, computational, and crystallographic study of the *N*-dialkyl *O*-arylcarbamate warhead

Anže Meden^a, Damijan Knez^a, Xavier Brazzolotto^b, Fabrice Modeste^c, Andrej Perdih^{a,d}, Anja Pišlar^e, Maša Zorman^a, Milica Denic^b, Stane Pajk^a, Florian Nachon^b, Stanislav Gobec^{*a}

^a*University of Ljubljana, Faculty of Pharmacy, Department of Pharmaceutical Chemistry. Aškerčeva 7, SI-1000 Ljubljana, Slovenia.*

e-mail: stanislav.gobec@ffa.uni-lj.si

^b*Institut de Recherche Biomédicale des Armées, Département de Toxicologie et Risques Chimiques, Unité Neurotoxiques. 91223 Brétigny sur Orge, France.*

^c*Institut de Recherche Biomédicale des Armées, Département des Plateformes et Recherches Technologiques, Unité Développements Analytiques et Bioanalyse. 91223 Brétigny sur Orge, France.*

^d*National Institute of Chemistry, Hajdrihova ulica 19, SI-1000 Ljubljana, Slovenia*

^e*University of Ljubljana, Faculty of Pharmacy, Department of Pharmaceutical Biology. Aškerčeva 7, SI-1000 Ljubljana, Slovenia.*

Abstract

Beside reversible butyrylcholinesterase inhibitors (BChEIs), a plethora of covalent ones, typically pseudo-irreversible carbamates, have been reported in literature. For the latter, however, in most cases the proper confirmation of their covalent mode of action is lacking. Additionally, the available reports on the structure-activity relationships of the *O*-arylcarbamate warhead are incomplete. Therefore, a follow-up on a series of pseudo-irreversible covalent carbamate human butyrylcholinesterase inhibitors (hBChEIs) and the structure-activity relationships of the *N*-dialkyl *O*-arylcarbamate warhead is presented. The covalent mechanism of binding was tested by IC₅₀ time-dependency profiles, and sequentially and increasingly confirmed by kinetic analysis, whole protein LC-MS, and crystallographic evidence. The computational studies provided valuable insights into the steric constraints and identified problematic, bulky carbamate warheads that could not reach and carbamoylate the catalytic Ser198. QM calculations lent further evidence that the steric effects seemed to be a key factor

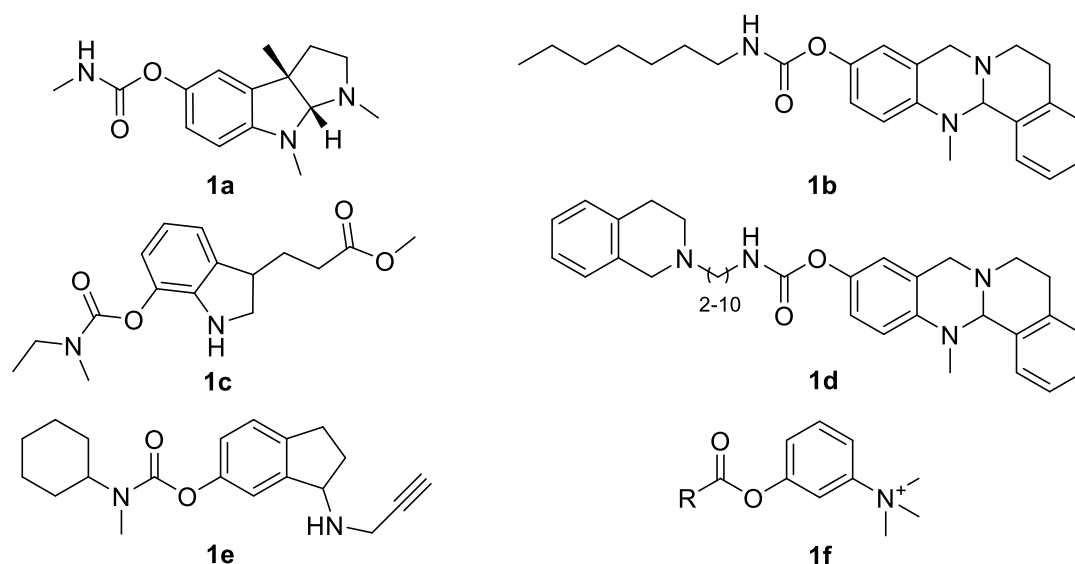
in determining the covalent binding behaviour of these carbamate ChEIs and their duration of action. Furthermore, the introduction of a clickable terminal alkyne moiety into one of the carbamate *N*-substituents and *in situ* derivatization with an azide-containing fluorophore enabled fluorescent labelling of plasma hBChE. This proof-of-concept study highlighted the potential of this novel approach and these compounds to be further developed as clickable molecular probes for investigating tissue localization and activity of ChEs.

Keywords: cholinesterase inhibitors, carbamoylation, butyrylcholinesterase, carbamate, pseudo-irreversible inhibition

Introduction

In addition to the well-known acetylcholinesterase (AChE), another enzyme capable of terminating cholinergic transmission is present in the human body, human butyrylcholinesterase (hBChE).¹ Because of its lower substrate specificity, hBChE is able to hydrolyse a number of different esters – e.g., hunger-hormone ghrelin, cocaine, heroin, etc., but its precise physiological role still remains a mystery. In the last three decades, BChE has emerged as an interesting and well-explored target in the medicinal chemistry community, especially in the fields of neurodegenerative diseases (predominantly Alzheimer's disease), bioscavenging organophosphorous nerve agents, inactivation of cocaine, heroin overdose prevention, and ghrelin-mediated effects on body weight.^{1–9} The enzyme's active site can be separated into several defined regions: the catalytic triad (Ser198, His438, Glu325), the oxyanion hole (Gly116, Gly117, Ala199), the choline-binding pocket (Trp82), and the acyl-binding pocket (Trp231, Leu286, Val288, Phe329). Near the entrance to the active site gorge is located the putative peripheral site, made of residues Asp70 and Tyr332.^{1,2}

Leaving a superabundance of classic reversible butyrylcholinesterase inhibitors (BChEI) aside, different cholinesterase inhibitor (ChEI) classes featuring carbamate moiety were reported in literature – e.g., derivatives of physostigmine (**1a**, *Scheme 1*), isosorbide, tetrahydroquinazoline (**1b**, **1d**), phenothiazine, xanthone, chalcone, coumarin, resveratrol, *N*-substituted piperidine and piperazine, indole (**1c**), etc., and were well-covered in a recent review highlighting their potential multifunctionality.¹⁰ Furthermore, the first discovered ChEI was indeed the plant alkaloid physostigmine, whose covalent pseudo-irreversible mechanism of action through a carbamate warhead was only later realized.¹¹



Scheme 1: Representative carbamate ChEI from literature.

The introduction of a carbamate warhead (most often the ethylmethyl carbamate of rivastigmine¹² as in **1c** or phenyl carbamate) on a variety of scaffolds easily produces BChEIs. However, a word of caution: especially in the field of cholinesterases, the literature is filled with examples of “IC₅₀-value-only” ChEIs that lack a proper confirmation of their covalent mode of action. Taking advantage of the BChE’s broad substrate recognition and promiscuous binding due to the large, hydrophobic active site, such compounds can easily bind reversibly with micromolar affinity. An example from our research group¹³ nicely shows that the presence of the carbamate moiety in a BChE-active compound does not simply guarantee a covalent mechanism of action. As with all the other covalent inhibitors, the carbamate inhibitors must be carefully optimized, too, both in terms of electrophilicity and reactivity of the warhead itself, and with regards to the correct orientation and steric requirements that allow for the covalent modification to proceed.^{14–19}

Although IC₅₀ values do not allow for a proper characterization of covalent inhibitors, within the series of compounds, comparing the ligands’ IC₅₀ values at the fixed timepoint can be both valid and faster than determining the exact k_{inact}/K_i values for a fast-moving drug discovery program.²⁰ In our hands, the following “triage” of testing potential covalent inhibitors is used: the IC₅₀ values are determined at different timepoints to ascertain the time-dependency profile (the decreasing IC₅₀ values with longer preincubation time are indicative of a special mechanism of binding²¹), the hits with pronounced or inconclusive time-dependent profile are then confirmed by kinetic analysis (*via* k_{obs} from initial velocity measurements^{22–24} or full

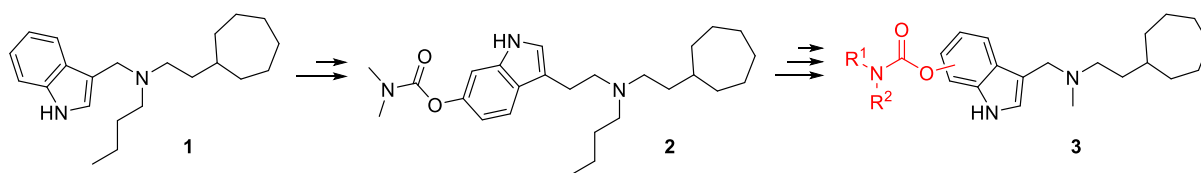
progress curve analysis²⁵), while the final unequivocal proof is provided by crystallization or LC-MS, or both.

To date, only a handful of studies investigated the structure-activity relationship and kinetic characterization of pseudo-irreversible carbamate ChEIs, with earlier efforts focused on the isocyanate-derived monosubstituted aryl carbamate, such as physostigmine (**1a**) derivatives.^{26,27} The Decker group has repeatedly reported on a series of evodiamine-derived BChEIs that among other interesting properties also feature a monosubstituted carbamate warhead. Beside the representative *n*-heptyl carbamate **1b**^{28,29}, *N*-monosubstituted carbamates with a terminal basic heterocyclic or tertiary amine (e.g., **1d**, *Scheme 1*) on a 2–10 carbon atom spacer had an extended duration of action (1–28 h), which was attributed to the interaction of the ω -moiety interacting with the peripheral site.²² Groner et al. have shown on two series of disubstituted *N*-alkyl-*N*-methyl carbamates with two different leaving group scaffolds that carbamoylation rates of hAChE are mainly influenced by the size and number of degrees of freedom of the *N*-alkyl (R) substituent, while for hBChE, the rates were more dependent on the structure of the leaving group. Decarbamoylation rates were greater for hBChE than for hAChE and also less dependent on the size of R. For hBChE, the dimethylcarbamoylated enzyme recovered the fastest. Interestingly, the bulkier *N*-cyclohexyl-*N*-methyl carbamate **1e** was inactive.²³ The temperature also had a substantial impact on decarbamoylation rate.¹² For AChE, Venkatasubban and coworkers reported on a series of monomethyl, dimethyl, ethyl methyl and diethyl carbamates with different leaving groups (phenols, fluoride). Due to long recovery times (up to several weeks), radiolabeling the hAChE and calculation of the final substrate turnover rate was necessary to accurately determine the decarbamoylation constants within a reasonable timeframe (up to 24 h). The increase in carbamate size by adding additional *N*-methyl or *N*-ethyl groups had a significant impact on the decarbamoylation rates of **1f**, with the approximate ratios H₂N : MeNH : Me₂N : EtMeN : Et₂N = 8000 : 800 : 200 : 10 : 1.³⁰

Moreover, AChE and BChE can be used as biomarkers for the detection of Alzheimer's disease^{1,31,32}, Hirschsprung's disease^{33,34}, and multiple sclerosis.^{35,36} To date, only a few AChE^{37–42} and BChE^{43–45,45–47} fluorescent probes and histochemical methods⁴⁸ enable tissue ChEs location and activity determination. Accordingly, the development of new chemical probes for investigating the roles of ChEs in physiological and pathophysiological processes *in vitro* and *ex vivo* is required by biologists and neurobiologists.^{49–51}

In the previous publication⁵⁷ we reported the successful conversion of tryptophan-derived *sp*³-rich selective hBChE inhibitors into pseudo-irreversible inhibitors by introducing a carbamate

moiety that enabled covalent binding to the target and prolonged inhibition (*Scheme 2*). In this work, we follow up on this series of pseudo-irreversible covalent carbamate hBChE inhibitors and report on their structure-activity relationship, selectivity, and their potential to be used as clickable molecular probes for the fluorescent labelling of ChEs.

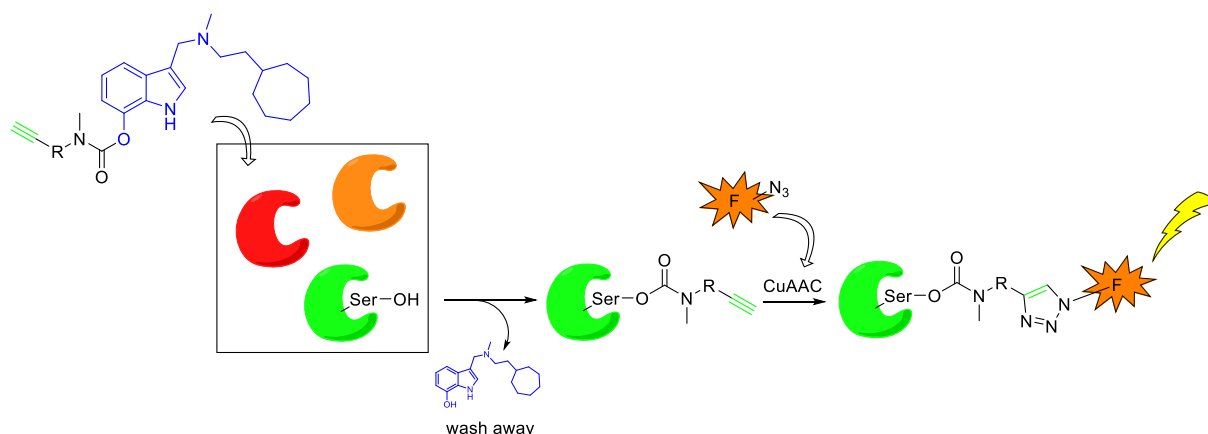


Scheme 2: Conversion of reversible selective hBChE inhibitor **1** scaffold⁵⁷ to a pseudo-irreversible covalent carbamate inhibitor **2**⁵⁷ and the structure-activity relationship of the carbamate warhead (general structure **3**).

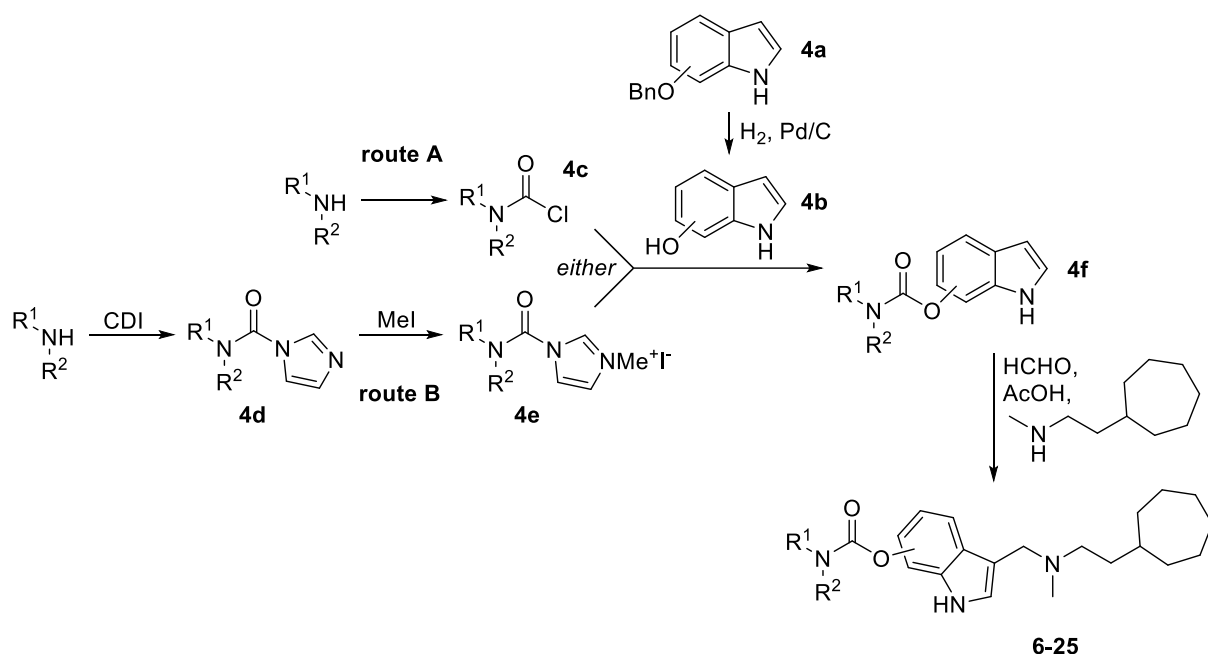
Design and Chemistry

Noncovalent fluorophore-labelled ChEIs have significantly lower affinity and specificity towards ChEs, because fluorophore usually does not contribute significant new interactions with the active site. A substantial portion of the fluorophore is free and in equilibrium with the bound inhibitor in the active site. Additionally, it can bind to tissue samples in a nonspecific manner. The former is responsible for high background fluorescence and the latter for artefacts in the microscopy imaging.

To improve the selectivity of probes, the following approach could be used that has not yet been reported in the literature: a “clickable” moiety (i.e., alkyne) at the carbamate warhead is transferred and pseudo-irreversibly bound in the ChEs’ active site, while the unbound inhibitor and the leaving group can be effectively removed by washing, leaving only the “clickable” alkyne^{52,53} on the protein of interest to be labelled in the next step *via* the copper(I)-catalyzed click reaction (Copper-Catalyzed Azide-Alkyne Cycloaddition, CuAAC) with an azide-functionalized fluorophore (*Scheme 3*). *In situ* click chemistry has already been proven as a valuable tool in the discovery of potent AChE inhibitors.^{54–56}



Scheme 3: The proposed labelling of ChEs with a carbamate warhead and subsequent CuAAC click derivatization with a fluorophore.



Scheme 4: General synthetic route from disubstituted amines to carbamate end compounds.

The required, air-sensitive 6- or 7-indolols **4b** were prepared *ex tempore* from commercially available benzyloxyindoles **4a** through hydrogenolytic debenzylation. Seemingly straightforward carbamoylation with carbamoyl chlorides **4c** (route A, *Scheme 4*) in presence of different bases led to a mixture of products. Presumably C3-alkylation is facile, as well, due to the electron-rich character of these indolols. Therefore, a cleaner alternative was sought – route B *via* *N,N*-dialkylcarbamoylimidazolium⁵⁸ salts **4e** in presence of *N,N*-diisopropylethylamine (DIPEA) afforded only the desired *O*-carbamoylated product **4f**. This route offers additional advantages, for instance, the greater commercial availability of disubstituted amines *vs.* carbamoyl chlorides, it avoids the use of highly toxic (di-, tri-

)phosgene, and is also exceptionally mild and therefore suitable for sensitive or polyfunctional amines (e.g, as in **21**, **22**). The final compounds were then easily prepared in one additional step – Mannich reaction of indole carbamates **4f** with formaldehyde and 2-cycloheptyl-*N*-methylethan-1-amine in acetic acid at room temperature. This last reaction step was carefully chosen to allow for gentle reaction and isolation conditions – namely, the absence of strong acids or bases, which could destroy labile electrophilic warheads.

Results and discussion

Inhibition of cholinesterases

The reversible inhibitor scaffold that was optimal in terms of potency and selectivity was retained from the previous series⁵⁷, only the *n*-butyl substituent on the central amine was replaced by a methyl group to balance the lipophilicity (*Scheme 2*). We have already established that positions 6 and 7 on the indole ring are suitable for the introduction of the carbamate warhead, therefore only 6- and 7-substituted indolyl carbamates were designed and compared (*Tables 1–3, Figures 1, S1–2*).

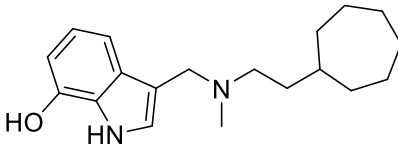
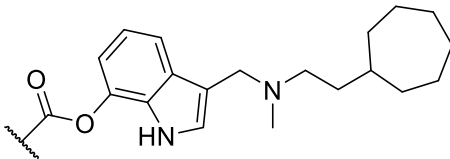
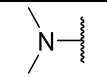
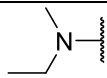
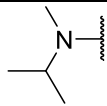
As expected, the leaving group for 7-substituted indolyl carbamates, **5**, had a decreased inhibitory potency compared to deshydroxy analogues⁵⁷, since the polar 7-hydroxy group occupies the highly lipophilic acyl-binding pocket (*Table 1*). The archetypal dimethyl carbamate **6** had single digit nanomolar affinity and a roughly 300-fold higher selectivity for hBChE over hAChE. Replacing one of the methyls with larger substituents – e.g., ethyl in **7**, isopropyl in **8**, *tert*-butyl in **9**, benzyl in **10**, led to decreased potency, except in the case of benzyl methyl carbamate **10**, where the benzyl group likely favourably interacts with aromatic residues either in the acyl- or choline-binding pocket. The increased steric bulk of **9** *tert*-butyl precluded the carbamoylation of the catalytic Ser198. Increasing the steric repulsion further, the diethyl analogue **11** had approximately 30 times decreased affinity vs. parent compound **6**, however it selectively carbamoylated only hBChE (*Figure 1*). The selectivity factor for hAChE was only 90, nevertheless the differential duration of action intertwined with PD-PK processes could be worth exploring further. The bulkiest diisopropyl carbamate **12** lost the ability to carbamoylate either of ChEs. Locking the flexible diethyl substituent in a six membered ring (**13**, **14**) decreased the steric factors back to the level of ethyl methyl carbamate.

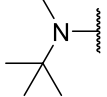
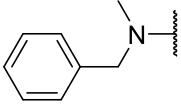
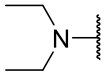
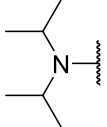
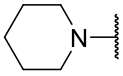
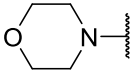
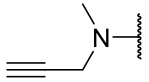
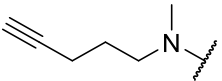
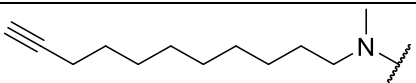
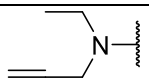
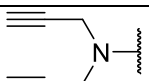
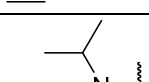
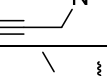
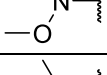
With a possibility of click derivatization and fluorescent labelling of hBChE in mind, we also introduced a terminal alkyne into one of the carbamate substituents – e.g., replaced Me with

propargyl in **15**, pent-4-yn-1-yl in **16**, and undec-10-yn-1-yl in **17**. This led to clickable analogues with steric demands comparable to **7**, with **17** benefitting from additional van der Waals interactions. The increased steric bulk might have shifted the selectivity profile completely towards hBChE, as in **11**, therefore, compounds **18**, **19**, and **20** with ethyl, propargyl, and isopropyl propargyl carbamate moiety were synthesized and tested. However, the selectivity factor did not exceed 350.

Since both carbamoylation and decarbamoylation are dependent on both steric and electronic factors, two other interesting analogues were prepared, with methoxy (**21**) and dimethylamino (**22**) substituent on the carbamate nitrogen (*Table 1*). The electron-withdrawing character of these substituents should increase both de- and carbamoylation rates. In fact, when we tried to ascertain the rate constants through k_{obs} measurements, the fast reactivation precluded the separation of carbamoylation and decarbamoylation phases. Therefore, these two compounds are better described as slow substrates.

Table 1: *In vitro* ChE inhibitory potencies of 7-substituted indolyl carbamates (compounds **6**–**22**) and their leaving group (compound **5**).

| Structure | Compound | hBChE | hAChE |
|--|----------|---|--------------|
| | | IC ₅₀ ± SEM [nM] ^a 5 min preincubation | |
| | | time-dependency observed: yes/no | |
|  | 5 | 373.3 ± 53.1 | 11593 ± 2676 |
| General structure:  | | | |
|  | 6 | 1.76 ± 0.04 | 558.6 ± 98.7 |
| | | yes | yes |
|  | 7 | 10.41 ± 2.99 | 6816 ± 1261 |
| | | yes | yes |
|  | 8 | 114.2 ± 15.3 | 2833 ± 346 |
| | | yes | yes |

| | | | |
|---|-----------|-------------------|------------------|
|  | 9 | 147.0 ± 9.0 | 10042 ± 2183 |
| | | no | no |
|  | 10 | 11.59 ± 1.76 | 531.2 ± 16.9 |
| | | yes | yes |
|  | 11 | 60.95 ± 5.95 | 5590 ± 374 |
| | | yes | no |
|  | 12 | 230.1 ± 30.9 | 4629 ± 724 |
| | | no | no |
|  | 13 | 5.28 ± 0.55 | 529.1 ± 45.6 |
| | | ambiguous | yes |
|  | 14 | 11.42 ± 0.56 | 3584 ± 1182 |
| | | ambiguous | yes |
|  | 15 | 7.75 ± 1.45 | 340.3 ± 20.2 |
| | | ambiguous | yes |
|  | 16 | 12.29 ± 2.01 | 1081 ± 65 |
| | | yes | yes |
|  | 17 | 3.773 ± 0.804 | 123.2 ± 17.9 |
| | | yes | yes |
|  | 18 | 21.94 ± 3.49 | 7526 ± 1047 |
| | | yes | yes |
|  | 19 | 32.75 ± 3.18 | 464.1 ± 38.2 |
| | | ambiguous | yes |
|  | 20 | 80.49 ± 15.51 | 5354 ± 994 |
| | | no | no |
|  | 21 | 157.9 ± 16.05 | 1101 ± 130 |
| | | ambiguous | no |
|  | 22 | 13.15 ± 3.40 | 5560 ± 1029 |
| | | yes | yes |

^a SEM – standard error of the mean, data are the average of two independent experiments, each performed in triplicate.

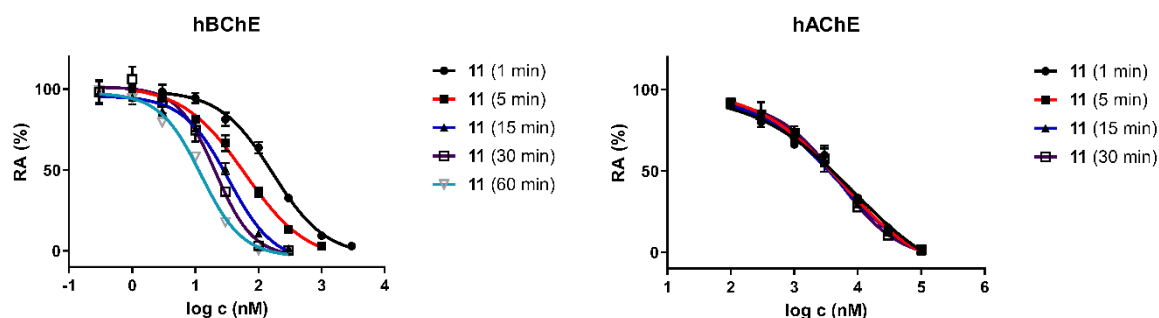


Figure 1: Time-dependency experiments on hBChE (left) and hAChE (right) for diethyl carbamate inhibitor **11**. The residual activities (RA) are plotted against log-concentration. The leftward shift – the decreasing of IC_{50} values with longer preincubation time – suggests the covalent mechanism of inhibition, as in case of hBChE (left). Data from other time-dependency experiments can be found in Supporting Information.

To better understand the steric factors, which affect the covalent mechanism of action, we also tested the fragment-sized synthesis intermediates **6a**, **7a**, **12a**, and **14a** (Table 2, Figure S2). The fragments displayed non-negligible reversible binding affinity, as seen in **12a** and **14a**. The latter is especially interesting since it lacks the pseudo-irreversible inhibition character of the full-sized inhibitor **14**, which shows that the rest of the molecule that directs the warhead in an appropriate position using reversible interactions can be equally important factor that governs the activity of covalent inhibitors.⁵⁹

Table 2: *In vitro* ChE inhibitory potencies of carbamate fragments.

| Structure | Compound | hBChE $IC_{50} \pm SEM [\mu M]^a$ 30 min preincubation | hAChE RA ^b at 100 μM after 30 min preincubation |
|-----------|------------|--|---|
| | | time-dependency observed: yes/no | |
| | 6a | 1.66 ± 0.09 | $2.4 \pm 0.6\%$ |
| | | yes | yes |
| | 7a | 1.39 ± 0.06 | $56.2 \pm 5.4\%$ Not active |
| | | yes | |
| | 12a | 12.78 ± 3.42 | $66.5 \pm 5.6\%$ Not active |

| | | | |
|--|------------|-----------------|------------------|
| | | no | |
| | 14a | 2.39 ± 0.91 | $19.3 \pm 1.3\%$ |
| | | no | ambiguous |

^aSEM – standard error of the mean, data are the average of two independent experiments, each performed in triplicate.

^bRA – residual activity (mean \pm standard deviation of one independent experiment performed in triplicate).

In an effort to design a selective covalent carbamate hBChE inhibitors, we prepared also a series of 6-substituted indolyl carbamates, since this approach has been successful before.⁵⁷ The dimethyl carbamate **23** inhibited both ChEs and had a decreased potency compared to the 7-substituted analogue **6**. Increasing the steric bulk led to compounds that lost the ability to covalently modify the enzyme (*Table 3*).

Table 3: *In vitro* ChE inhibitory potencies of 6-substituted indolyl carbamates (compounds **23**–**25**).

| General structure | | Compound | hBChE | hAChE |
|---|-----|-----------|---|--------------|
| <div> <div>R²</div> <div>R¹</div> </div> <div> <div>R¹=</div> <div>R²=</div> </div> | | | IC₅₀ ± SEM [nM]^a 5 min preincubation | |
| | | | time-dependency observed: yes/no | |
| | | | Me | Me |
| | | yes | yes | |
| iPr | iPr | 24 | 86.23 ± 18.04 | 336.5 ± 37.8 |
| | | | no | no |
| propargyl | Me | 25 | 10.15 ± 2.15 | 1456 ± 138 |
| | | | no | no |

^aSEM – standard error of the mean, data are the average of two independent experiments, each performed in triplicate.

To support the covalent mechanism of binding with kinetics evidence, the carbamoylation rate constant (k_{carb}) and inhibitory constant for the reversible binding K_i were determined for **6** from

pseudo-first order inhibition rates (k_{obs}) (Figure 2, Table 4). The carbamate reversibly binds with low nanomolar affinity to the enzyme before the carbamoylation takes place.

Decarbamoylation rate constants at room temperature were determined by following the recovery of the diluted inhibited enzyme (Figures 2, S3) and are presented in Table 4. The rates translate to half-lives that span from 13 h for dimethyl carbamate **6** to 13 days for diethyl analogue **11** and to Gibbs activation energies on the scale of 24–25 kcal/mol. Increasing the size of one of the carbamate substituents to pent-4-yn-1-yl or benzyl, prolonged the duration of inhibition to approx. 2 and 4 days, respectively. The decreased steric demands and degrees of freedom in case of dipropargyl **19** vs. diethyl carbamate shortened the half-lives for almost 30 times, comparable to the dimethyl carbamate **6**. This data agrees with the one obtained by progress curve analysis on a same-scaffold BChEI from a previous series⁵⁷ and, with some extrapolation for different experimental conditions, the data on BChE²³ and AChE³⁰.

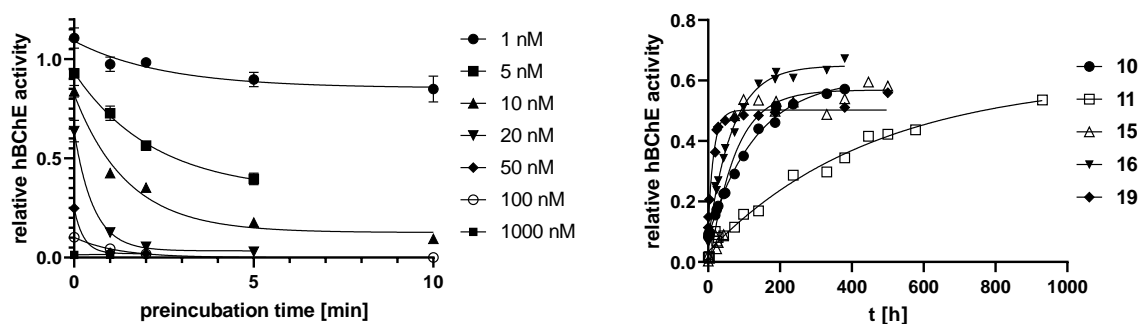


Figure 2: On the left, hBChE residual activity as a function of preincubation time at different **6** concentrations. The enzyme and inhibitor were preincubated for a specified amount of time, then the substrate was added, initial velocity measured, and compared with the uninhibited enzyme. Values are expressed as means \pm SEM of at least two duplicates. On the right, the reactivation of carbamoylated hBChE upon dilution for compounds **6**, **10**, **11**, **15**, **16**, **19**. The initial velocities were compared to uninhibited, identically diluted control enzyme solution.

Table 4: Carbamoylation of hBChE by **6** and reactivation of carbamoylated hBChE – kinetic parameters.

| Compound | Concentration [nM] | k_{obs} [min^{-1}] | R^2 goodness of fit |
|----------|--------------------|--|--------------------------|
|----------|--------------------|--|--------------------------|

| | | | | |
|-----------|---|----------------------------|---|--------|
| 6 | 5 | 0.4475 | | 0.9845 |
| | 10 | 0.6765 | | 0.9728 |
| | 20 | 1.855 | | 0.9871 |
| | 50 | 3.752 | | 0.9993 |
| | R² for double reciprocal plot: | | | 0.9608 |
| | K_i [nM] | 1.05 | | |
| | k_{carb} [M⁻¹ × min⁻¹] | 10.635 | | |
| | k_{decarb} [h⁻¹] at 25 °C | t_{1/2} [h] | Eyring ΔG[‡] [kcal/mol] | |
| | 0.05331 | 13.0 | 24.0 | 0.9982 |
| 10 | 0.007513 | 92.2 | 25.2 | 0.9950 |
| 11 | 0.002177 | 318.3 | 25.9 | 0.9872 |
| 15 | 0.01415 | 49.0 | 24.8 | 0.9133 |
| 16 | 0.01489 | 46.5 | 24.8 | 0.9943 |
| 19 | 0.06194 | 11.2 | 24.0 | 0.9768 |

Mass spectrometry study of BChE carbamoylation

To unequivocally confirm the covalent binding of the carbamate warhead to hBChE – i.e., the carbamoylation of catalytic Ser198, we conducted a mass spectrometry study. Since the bound carbamate moiety could be hydrolysed under pepsinolytic conditions that are typically used for sample preparation for MS, whole protein mass spectrometry analysis using recombinant hBChE produced in *E. coli*⁶⁰ was undertaken. The absence of glycosylation in a protein from prokaryotic expression system was needed to produce a uniform multicharged protein spectrum. The protein (in control and carbamoylated samples) eluted at 7.2 min under our experimental conditions and the deconvolution of spectra resulted in one major species for each sample.

For **14**, the native hBChE in the control sample featured a mass of 60069 ± 1 Da (ProtParam⁶¹ calculated mass from the primary sequence: 60069.2 Da), while the 20-min **14**-incubated sample produced a species with mass of 60183 ± 1 Da (*Figure 3*). This mass difference of 114 ± 1 Da, is in good accordance with the expected mass difference for the morpholinocarbamoylated hBChE (114.1 Da). Interestingly, injection of the same **14**-treated sample incubated for more than 60 min, showed only the presence of the free, non-carbamoylated hBChE, after deconvolution.

Similarly, for **6**, the native hBChE in the control sample featured a mass of 60073 ± 1 Da (4 Da difference to the ProtParam⁶¹ calculated mass) and the **6**-incubated sample produced a species

with mass of 60144 ± 1 Da (Figures 3, S4). The mass difference of 71 ± 1 Da, is in good accordance with the expected mass difference for the dimethylcarbamoylated enzyme (72.1 Da).

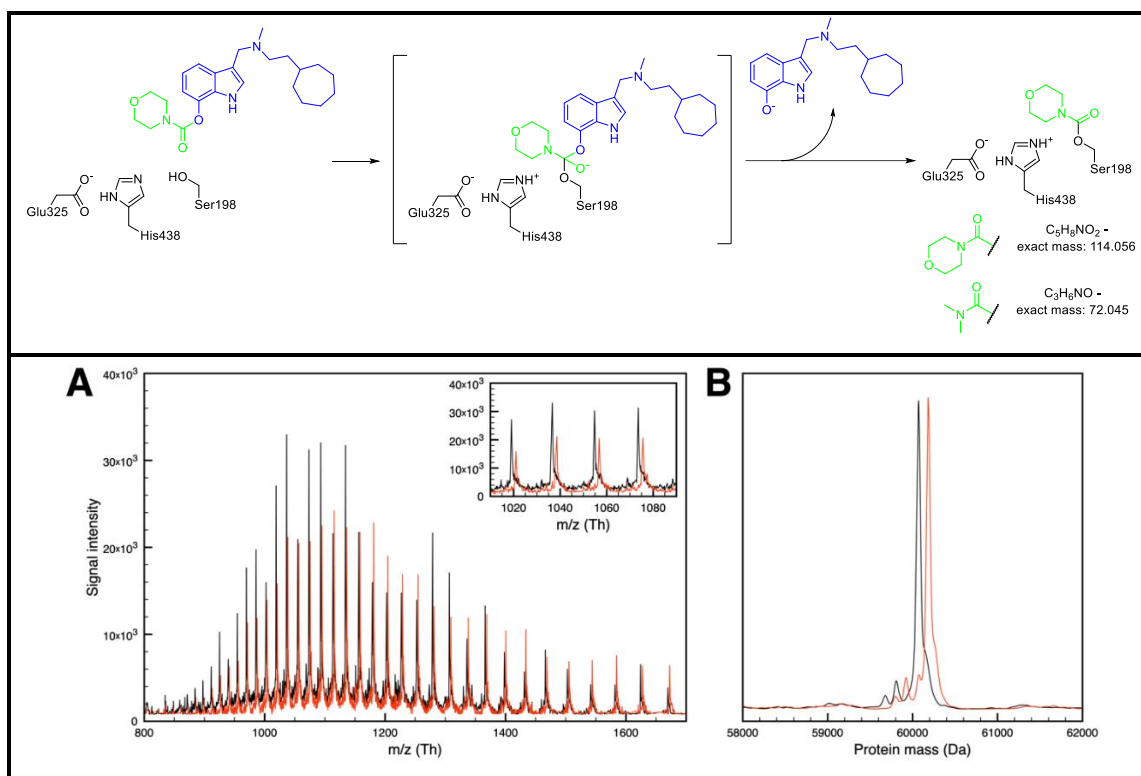


Figure 3: Above, carbamoylation of hBChE by carbamates **14** and **6**. The carbamoyl moiety is coloured green, the leaving group blue, and the enzyme black. Below, mass spectrometry analysis of hBChE carbamoylation by **14**. **A** – a characteristic protein spectra recorded at 7.2 min retention time together with a close view insert. **B** – deconvoluted spectra for control sample (black) and **14**-treated sample after 20 min (red).

Cytotoxicity

The compound **6** was also tested for cytotoxicity in SH-SY5Y and HepG2 cell lines, with IC_{50} values of $5.8 \mu M$ and $7.1 \mu M$, respectively (Figure 4). The substantial cytotoxicity of these compounds (observed at 1000-fold higher concentrations than IC_{50}) might be the result of unspecific binding due to the high lipophilicity of the scaffold. However, this work was only meant to explore the *N*-dialkyl *O*-arylcarbamate warhead, not to produce developable lead compounds. Thus, a chosen *O*-arylcarbamate warhead can still be installed on a less cytotoxic scaffold to reap the benefits of pseudo-irreversible inhibition.

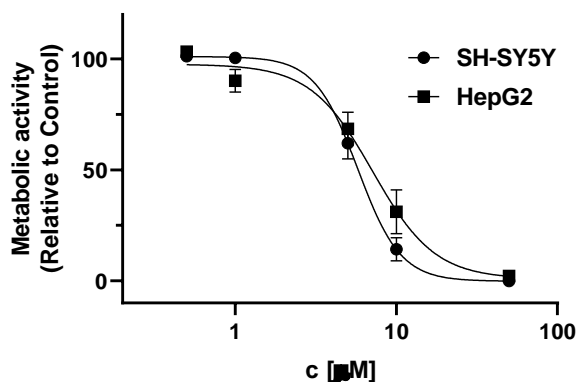


Figure 4: *In vitro* cytotoxicity profile for **6**. SH-SY5Y (●) and HepG2 (■) cells were incubated in the presence of increasing concentrations of compounds (1–50 μ M) in serum-reduced medium. After 48 h, the metabolic activity was evaluated using the MTS assay. The control group (DMSO) was considered as 100% cell viability. Data are means \pm SEM of at least two independent experiments, each carried out in quadruplicate.

Trial fluorescent labelling of hBChE

Because its brightness and excellent photostability, rhodamine B was chosen as a basis of the clickable fluorophore. Secondary amides of rhodamine B exist in a nonfluorescent spirocyclic form at neutral pH and transform into ring-opened fluorescent form at lower pH.⁶² To remove this impact of pH on fluorescence, a ω -azido tertiary amide **26** was prepared with 1-(2-azidoethyl)piperazine, which is not prone to spirolactamization and subsequent loss of fluorescence. Human plasma is reported to contain 3.5–9.3 mg/L (41–109 nM) BChE² and is therefore an excellent and readily available biological sample for labelling experiments. Three time-dependent carbamates inhibitors were chosen based on their potency, selectivity ratio, and decarbamylation rate. The stability of carbamates in aqueous solution was also checked and they were found to be stable for weeks under physiologically similar conditions (see Experimental Section, Table 6). The compounds were incubated with plasma, the whole samples were labelled using *in situ* click reaction with Cu^+ and **26**, and the mixture resolved using SDS-PAGE, as described under the Experimental Section. The proteins were transferred to a nitrocellulose membrane using Western blot to improve the fluorescent detection. Clearly visible fluorescent bands were present only in the sample labelled with the inhibitor **17** (Figure 5, arrow) within the expected mass range for hBChE (68 kDa). Additional immunostaining with anti-hBChE antibodies was performed (Figure 5, right), and the fluorescent band marked with an arrow was also detected by antibodies. The origin of the other fluorescent bands (except the

unreacted fluorophore at the bottom of the gel) is unknown, perhaps the carbamates also bound to other serine hydrolases present in the plasma, the plasma may be contaminated with haemolyzed red blood cells and therefore also with hAChE, etc. This requires further exploration, but for this proof-of-concept study, the fluorescent labelling of hBChE with clickable carbamates was tentatively confirmed.

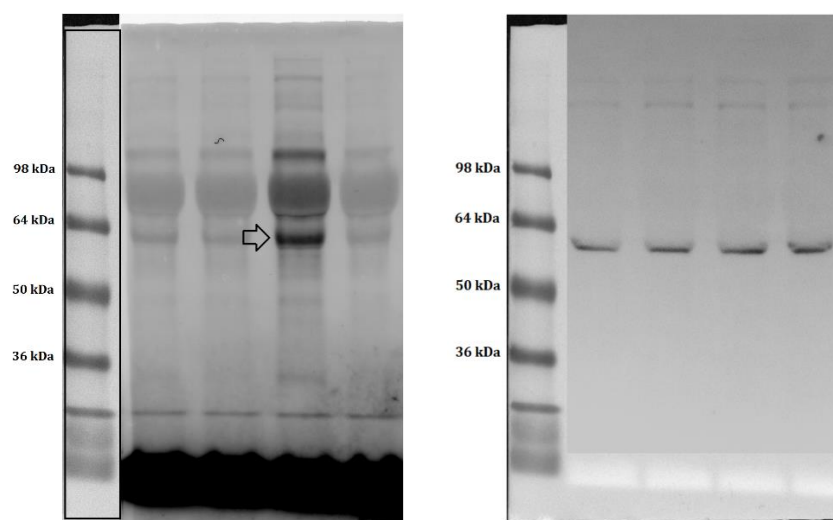


Figure 5: SDS-PAGE of plasma samples, labelled with carbamates. Lanes from left to right: protein ladder, control (MeOH-treated plasma), **16-**, **17-**, **18-**treated plasma. Left, the fluorescent detection at 595 nm; right, chemiluminescent detection of immunostained hBChE (predicted band signal at 68 kDa). The protein ladder standard was invisible under fluorescent and chemiluminescent detection, therefore it was detected under visible light and the pictures were overlaid.

Structural studies

To unambiguously confirm the covalent binding of carbamates to the catalytic serine, **6** as a representative, potent time-dependent hBChE inhibitor was selected for crystallization. After some trial-and-error, the careful selection of the crystal soaking conditions successfully led to the crystal structure of the dimethylcarbamoylated hBChE together in complex with the leaving group **5** at the 2.14-Å resolution (PDB 8AI7, *Figure 6, left*). Continuous electron density is observed close to Ser198 and the carbamate moiety, modelled here as a dimethylformamide molecule, can be fitted with a Ser198-O γ DMF-carbon distance of 1.4 Å, in accordance with the formation of a covalent bond. While there are some similarities in the binding mode to the compounds from the previous series⁵⁷ – i.e., the cation- π interaction of the central tertiary amine of the leaving group with Tyr332, and a hydrophobic region above Trp82 in the choline-binding pocket that is occupied by the cycloheptyl ring, the indole moiety is this time predominantly

facing the solvent (*Figure 6, right*). The reason for this is probably the steric hindrance with the dimethylcarbamoylated Ser198, where the methyl substituents encroach into the acyl-binding pocket that was previously occupied by a heterocyclic ring. The carbamoyl oxygen is nicely situated within the oxyanion hole, forming all three available hydrogen bonds with backbone amide hydrogens of Gly116, Gly117, and Ala199. Below His438 (modelled as protonated) and only 3.1 Å away from the carbonyl carbon of the dimethylcarbamate moiety is located a water molecule (water 188), which is appropriately positioned to affect the hydrolysis and regeneration of the catalytic residue.

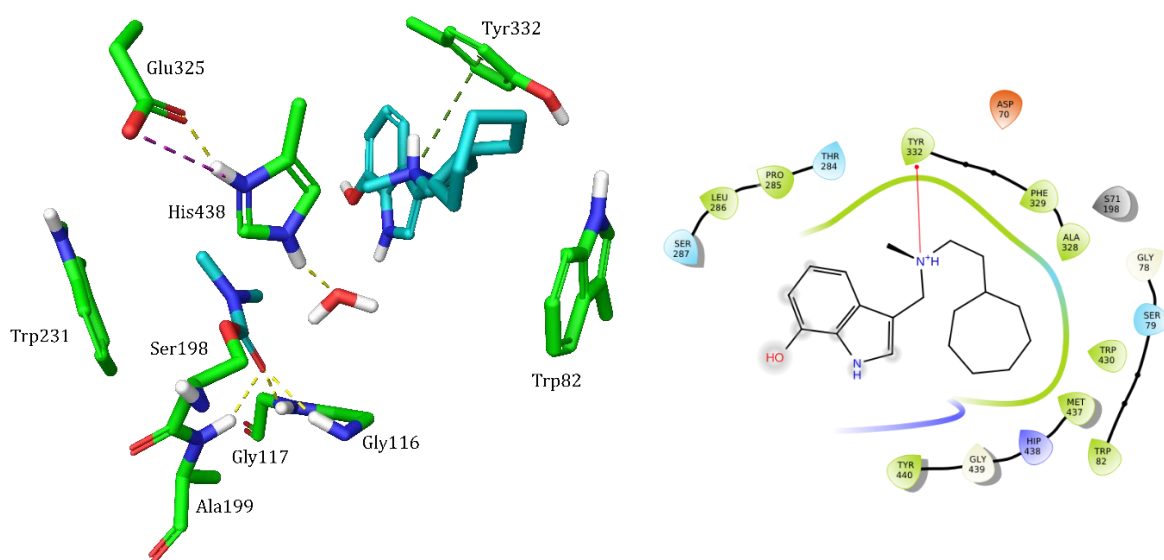


Figure 6: On the left, the crystal structure of **5** in complex with dimethylcarbamoylated human BChE (PDB 8AI7). The key amino acid residues are shown as green sticks, while **5** leaving group and dimethylcarbamoyl moiety on Ser198 are teal-coloured. The hydrogen bonds are shown as yellow dashed lines, cation- π interaction with Tyr332 as dark green dashed line, and salt bridge within the triad with magenta dashed line. Crystal water 188 is located 3.1 Å from the carbonyl carbon in an appropriate position to hydrolyse the carbamoylated catalytic Ser198. On the right, ligand interaction diagram for **5** leaving group in the carbamoylated hBChE active site. The cation- π interaction of the central tertiary amine with Tyr332 is shown as a red line. The cycloheptyl still occupies the hydrophobic region above Trp82 in the choline-binding pocket, while the indole was displaced from the acyl-binding pocket and is predominantly facing the solvent (grey circles denote the solvent exposure).

Computational studies

To further study the binding properties of our compounds and discern differential steric effects across the series of compounds, only the 7-substituted indolyl carbamates were studied *in silico*.

To be able to generate noncovalent docking poses that were in line with the known SAR, as well as the available structural data on this series of ligands (e.g., the crystal position of the cycloheptyl ring), several constraints had to be introduced (see Experimental section) and finally two predominant binding modes (case *A* and *B*) were identified.

In case *A*, the poses obtained had carbamate alkyls oriented towards the acyl-binding pocket, while in the case *B*, the poses obtained had carbamate alkyls oriented towards the choline-binding pocket (*Figure 7*). To decide which solution was more probable, binding pose metadynamics (*Figure S5*) and 1 μ s all-atom molecular dynamics (MD) simulations were performed for both cases. The metadynamics suggested that case *A* pose is more stable, however extended MD simulations revealed that both poses were unstable, as evident from the observed RMSD increase, broken hydrogen bonds with the oxyanion hole residues, as well as the disruption of the catalytic triad (*Figure 8A–F*). Namely, visual inspection revealed that in both cases, the carbonyl of the carbamate moiety that has resided in the oxyanion hole, underwent a 180 ° rotation (after 50 and 250 ns, respectively) and that the molecule distanced itself from the catalytic Ser198, thus preventing a covalent reaction. This instability of the prereaction poses suggests that this ligand does not prefer the short-lived non-covalent position, consistent with the experimentally observed non-covalent inhibition for this compound. It should be however noted that other factors, such as small changes in the protonation pattern of the charged binding site residues, the force field parameters used, as well as the utilization of the docking approach, which was optimized for noncovalent binding without steric conflicts, could also be important for the observed outcome.

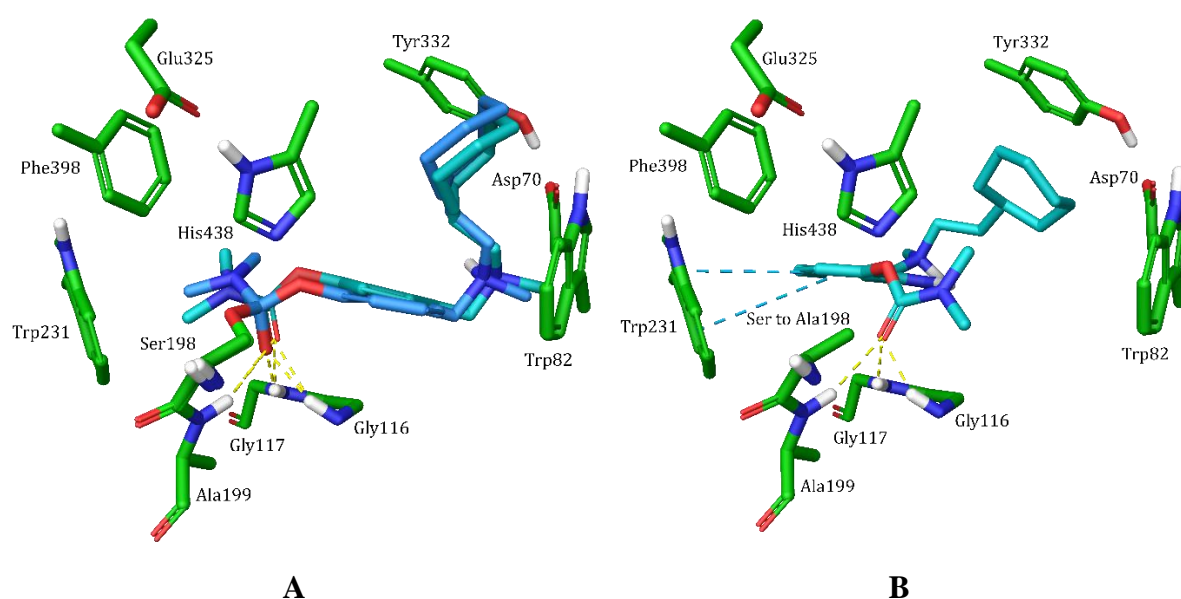


Figure 7: The two determined docking poses of **6** in the hBChE active site. Left, overlay of the prereaction (azure sticks) and postreaction (teal sticks) poses for case *A*. Right, the prereaction (teal sticks) pose for case *B*. The distance between the (ex-)carbonyl carbon and O γ -Ser198 was 2.4 and 1.4 Å for prereaction and postreaction pose in case *A*, and 2.8 Å for prereaction pose in case *B*, respectively.

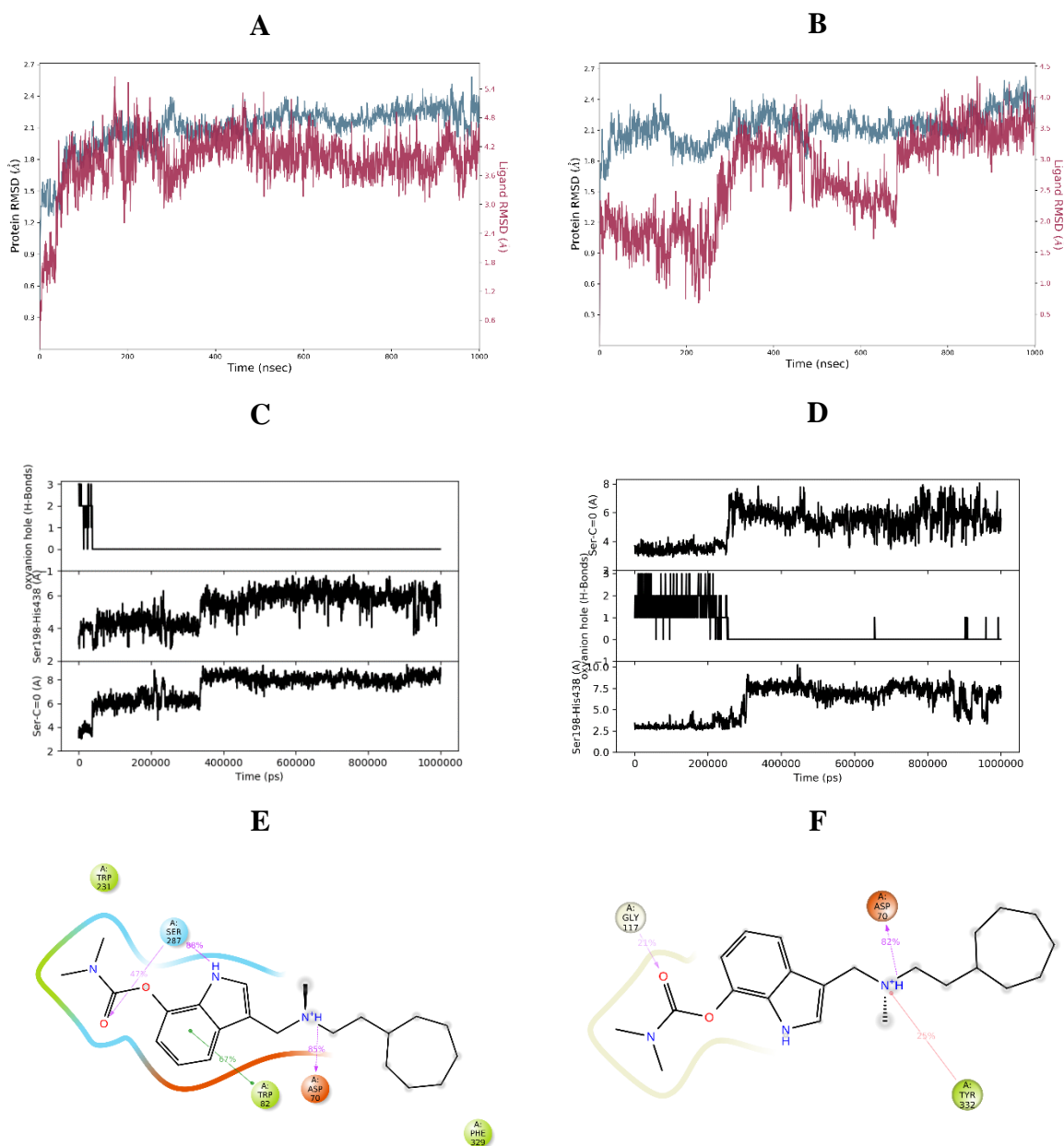
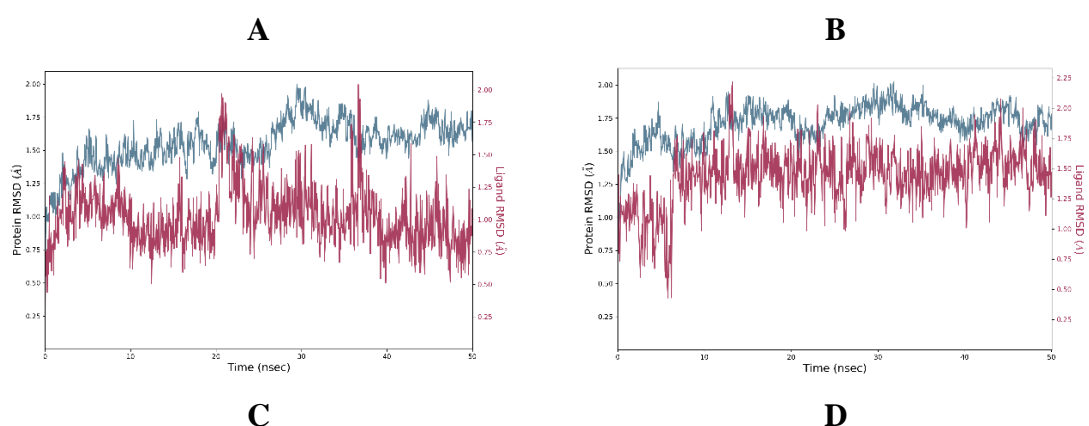


Figure 8A–F: Results of 1 μ s all-atom MD simulation of the noncovalent prereaction docking poses of compound **6**. The left figures belong to case *A* and the right ones correspond to case *B*. The first row (panels **A**, **B**) shows the RMSD plots over simulation time – the teal-coloured plot corresponds to the hBChE C α RMSD and the red-coloured to ligand RMSD values. For calculation of both parameters, all frames were first aligned to the backbone in the first,

reference frame. The second row (panels **C**, **D**) depicts the number of hydrogen bonds formed with the oxyanion hole residues (Gly116, Gly117, Ala199), the distance between Ser198 O γ and His438 N ϵ (in Å, indicating the stability of the triad), and the distance between Ser198 O γ and **6** carbonyl carbon (in Å, indicating the propensity for covalent bond formation). The third row (panels **E**, **F**) shows protein-ligand contacts and interactions that occur for more than 20% of the MD simulation time. The π - π interactions are shown as green lines, the cation- π interactions as red lines, hydrogen bonds are shown in blue and ionic interactions in magenta. Both poses are unstable in the long term, as evident from the RMSD increase, broken hydrogen bonds with the oxyanion hole residues, disruption of the catalytic triad. It is revealed upon visual inspection that in both cases, the carbonyl of the carbamate moiety that has resided in the oxyanion hole underwent a 180 ° rotation (after 50 and 250 ns, respectively) and that the molecule distanced itself from catalytic Ser198, preventing a covalent reaction.

Subsequently, we performed covalent docking calculations for compound **6**. Here, the observed poses seemed to favour the orientation of the carbamate alkyls towards the acyl-binding pocket (case A) exclusively. To provide insight into their stability, covalently bound postreaction poses from cases A and B (the later was manually generated) were evaluated in MD simulations. As evident from Figures 9A–F, the case A pose was substantially more stable, which was reflected in lower RMSD, persistent 3 hydrogen bonds with the oxyanion hole residues, stable catalytic triad (Ser198 O γ –His438 N ϵ distance approx. 3.3 Å), and overall, more interactions formed between the ligand and the binding site.



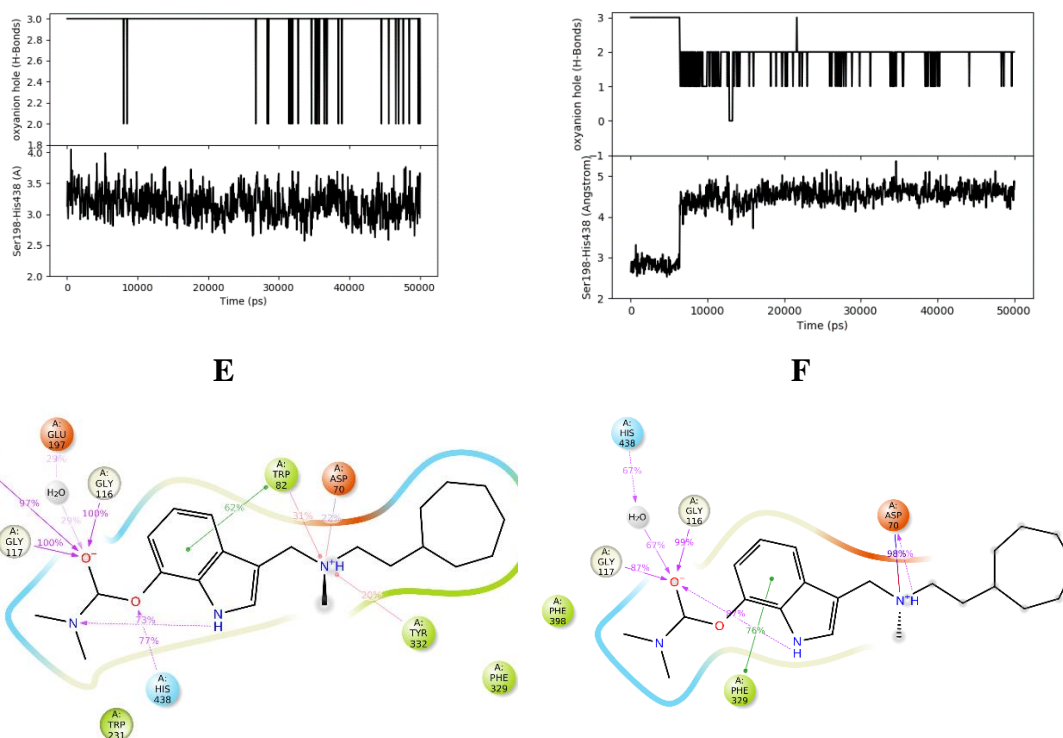
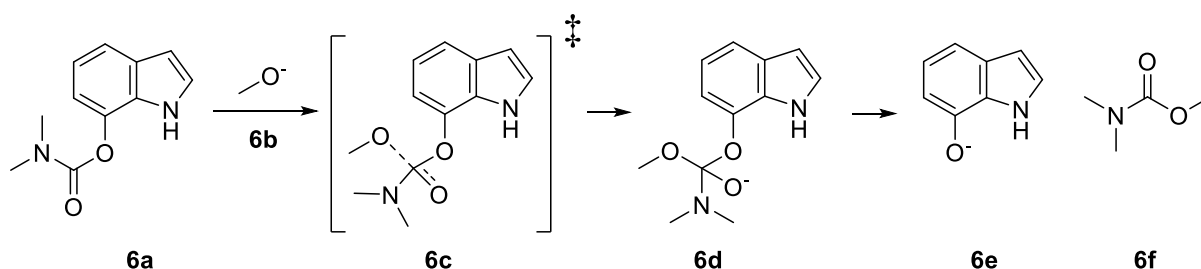


Figure 9A–F: The results from the MD simulation of the tetrahedral intermediate formed after the nucleophilic addition of Ser198 to the **6**'s carbamate carbonyl. The left figures correspond to a case A pose obtained with the CovDock covalent docking protocol and the right ones to a case B pose that was prepared by hand from a Glide pose where carbamate alkyls are oriented towards the choline-binding pocket. Please refer to Figure 8 for a detailed legend.

The results of the *in silico* covalent and noncovalent binding experiments indicated that that bound orientation described by case A, where the carbamate alkyl is oriented towards the acyl-binding pocket, is more probable for this series of compounds. Consequently, all the remaining 7-substituted indolyl carbamates were modelled in this way. From the pool of noncovalently docked molecules only **9**, **12**, **18**, and **20** with bulkier *N*-dialkyl substituents on the carbamate warhead produced no successful prereaction docking poses. Apart from **18**, these compounds displayed time-independent profile of reactivity in the *in vitro* assay, suggesting reversible binding only, in line with the docking results. Next, the covalent docking protocol successfully produced postreaction poses for all compounds except **12** and **20**, both having bulky carbamate warheads and exhibiting time-independent behaviour in the *in vitro* assay. The analysis of MD simulations of postreaction poses for time-independent, reversible **9** (Figure S6) showed that both poses were comparably stable within the given timeframe and exhibited a similar interaction profile.

The results of this computational work indicate that the steric factors in the prereaction pose must play a major role in determining reactivity, since the postreaction poses fitted the active site nicely, regardless of the carbamate *N*-alkyls' orientation. Furthermore, serious steric clash that prevents the carbamoylation of Ser198 was possible to predict using different docking techniques.

To further gain insight into the intrinsic chemical reactivity of the carbamate warhead and the electronic factors that govern the carbamoylation step, we used quantum mechanical (QM) calculations to approximately model the hydrolysis of **6** with a model nucleophile in solution. The investigated model reaction is outlined in Scheme 5: minimal representative structure, i.e., the fragment **6a** was used to reduce the size of the system, and methoxide as Ser198 surrogate. At the M06-2X/cc-pVTZ(-f)++//M06-2X/6-31G**++ level of theory DFT-predicted Gibbs activation free energy barrier ΔG^\ddagger was 20.9 kcal/mol. The reaction free energy up to the tetrahedral intermediate **6d** was 14.6 kcal/mol, while the corresponding energy for the complete reaction (**6a+6b** to **6e+6f**) was exothermic, -16.4 kcal/mol, respectively (Table S2). This reaction was modelled in implicit water solution without taking the enzymatic environment into account, which could be better described by QM/MM techniques. Even considering the inaccuracies connected with the DFT method, and that the enzymes by definition lower the reaction barrier, typically by stabilizing the transition state, the obtained reaction barrier was found to be in the same range as the experimentally determined Gibbs free energy of activation for **6**, 18.5 kcal/mol.



Scheme 5: The studied model reaction of **6a** with methoxide.

Altogether, these data suggest that the crucial factors that dictate the covalent mechanism of action within this series of carbamate ChEIs are the size and bulkiness of the carbamate *N*-dialkyl substituents. Significant steric clash prevents the approach to the catalytic Ser198, and efficient binding and activation by the oxyanion hole. The intrinsic reactivity of the warhead itself should be approximately the same for different carbamate *N*-dialkyl substituents and was found to be energetically comparable with the behaviour observed in solution.

Conclusion

In this work, we followed up on a series of pseudo-irreversible covalent carbamate hBChE inhibitors, determined the carbamate warhead structure-activity relationship and steric requirements/constraints for the carbamoylation of the catalytic Ser198 with dialkylcarbamoyl moieties. The covalent mechanism of binding was sequentially confirmed by IC₅₀ time-dependency profiles, kinetic analysis through k_{obs} determination and recovery-upon-dilution experiments, LC-MS, and finally by X-ray crystal structure determination. For the selected 7-substituted carbamate inhibitor **6**, the mass increase corresponding to the dimethylcarbamoyl moiety was observed in whole protein LC-MS experiment, and the crystal structure of dimethylcarbamoylated enzyme together in complex with the leaving group **5** was obtained – making this the first known crystal structure of the dimethylcarbamoylated BChE.

The computational studies provided valuable insight into the steric constraints and also tentatively identified problematic, bulky carbamate warheads that could not reach the catalytic Ser198 to affect the carbamoylation. Additionally, the determined carbamoylation rate and Gibbs free energy of activation for **6** agreed nicely with the quantum-mechanically predicted reaction barrier for reaction with a model nucleophile in solution. Therefore, the steric effects seem to be the crucial factor in determining the covalent binding behaviour of these carbamate ChEIs. These results bring the missing (and in our opinion, final) pieces to the puzzle on the carbamate ChEI and, translated across different scaffolds, could aid other researchers in selection of a proper carbamate structure that will achieve the desired, prolonged duration of action.

Furthermore, the introduction of a clickable terminal alkyne moiety into one of the carbamate substituents and *in situ* derivatization with an azide-containing fluorophore enabled fluorescent labelling of the enzyme, as was confirmed by the proof-of-concept study with plasma hBChE. This highlights the potential of this novel approach and these compounds to be developed as clickable molecular probes for investigating tissue localization and activity of ChEs.

Experimental

Inhibition of Cholinesterases

The inhibitory potencies of the compounds against the ChEs were determined using the method of Ellman following the procedure described previously.²¹ Briefly, compound stock solutions in DMSO were incubated with Ellman's reagent and the ChEs (final concentrations: 370 μM

Ellman's reagent, approximately 1 nM or 50 pM hBChE or hAChE, respectively) in 0.1 M sodium phosphate pH 8.0 for 5 min at 20 °C. For time-dependency measurements, the pre-incubation time was varied (1 min, 5 min, 15 min, 30 min or 60 min). The reactions were started by the addition of the substrate (final concentration, 500 μ M butyrylthiocholine iodide or acetylthiocholine iodide for hBChE and hAChE, respectively). The final content of DMSO was always 1%. The increase in absorbance at 412 nm was monitored for 2 min using a 96-well microplate reader (Synergy HT, BioTek Instruments, VT, USA). The initial velocities in the presence (v_i) and absence (v_o) of the test compounds were calculated. The inhibitory potencies were expressed as the residual activities, according to $RA = (v_i - b) / (v_o - b)$, where b is the blank value using phosphate buffer without ChEs. For IC_{50} determinations, at least seven different concentrations for each compound were used. The IC_{50} values were obtained by plotting the residual ChE activities against the applied inhibitor concentrations, with the experimental data fitted to a four-parameter logistic function (GraphPad Prism 9.4). Tacrine and donepezil were used as positive controls. The progress curves for the time courses of product formation for the hydrolysis of butyrylthiocholine were measured on an Agilent Cary 3500 UV-VIS spectrophotometer with Compact Peltier (thermostatted at 25 °C) at 412 nm using a 0.6 mL 0.5 cm cuvette. 30 mM Tris buffer pH 7.0 with 1 mg/mL BSA and 0.02% NaN_3 was used and all dilutions were done in glass vessels (note: dilute hBChE solutions rapidly lose activity, presumably due to adsorption to plastic, preventing meaningful decarbamylation assays. In our hands, under the above conditions only, the diluted and stock solutions of hBChE were stable for at least a month at room temperature.). Total volume in the cuvette was always 500 μ L, and enzyme solutions that gave upon dilution $v_o = (dA/dt) \approx 0.5$ (for carbamylation) and ≈ 1 for (for decarbamylation) were used. For carbamylation experiments, 0.5–1 μ L of enzyme stock, 5 μ L of compound solution, and 484 μ L of buffer were preincubated for the specified time, then 10 μ L of the mixture of 25 mM Ellman's reagent (DTNB) and 20 mM butyrylthiocholine (large excess to prevent substrate depletion) were added, quickly mixed, and measurement started. For decarbamylation experiments, 50 μ L of the enzyme stock solution and 0.25–0.5 μ L of the compound solution in MeOH (concentration chosen to achieve 85–95% inhibition, typically 0.5–1 mM) were incubated for 1 h at room temperature, then the mixture was diluted 1:1000 with the buffer, and 500 μ L aliquots were drawn at different timepoint, mixed with 10 μ L of the mixture of 25 mM Ellman's reagent (DTNB) and 20 mM butyrylthiocholine, and hBChE activity assayed. The data analysis followed the literature.^{23,29}

Experimental Gibbs free energy activation barrier ΔG^\ddagger was calculated from the (de)carbamoylation rates *via* the Eyring equation (taking reference concentration of 1 M, at 298.15 K).

Cytotoxicity

The human neuroblastoma SH-SY5Y and human liver carcinoma HepG2 cell lines were purchased from American Type Culture Collection (Manassas, VA, USA). Cells were cultured in Advanced Dulbecco's modified Eagle's medium (Gibco, Thermo Fisher Scientific, Waltham, MA, USA) supplemented with 10% fetal bovine serum (FBS, Gibco), 2 mM L-glutamine, 50 U/mL penicillin and 50 μ g/mL streptomycin (Sigma, St. Louis, MO, USA) in a humidified atmosphere of 95% air and 5% CO₂ at 37 °C, and grown to 80% confluence. Prior to cell treatment, complete medium was replaced with serum-reduced medium (*i.e.*, with 2% FBS). **6** was prepared as a 20 mM stock solution in DMSO. The cells were seeded in 96-well plates (2 \times 10⁴/well) and assessed by MTS ([3-(4,5-dimethylthiazol-2-yl)-5-(3-carboxymethoxyphenyl)-2-(4-sulfophenyl)-2H-tetrazolium, inner salt) assay for their response to **6**. Cells were treated with increasing concentrations of compounds (1–50 μ M) in serum-reduced medium, and metabolic activity was assessed after 48 h using the CellTiter 96[®] Aqueous One Solution Cell Proliferation Assay (Promega, Madison, WI, USA), in accordance with the manufacturer's instructions. Absorbance was measured with an automatic microplate reader (Tecan Safire², Switzerland) at a wavelength of 492 nm. Results are expressed as a percentage of the control (DMSO), and are representative of at least two independent experiments, each performed in quadruplicate, presented as means \pm SEM.

Trial fluorescent labelling of hBChE

EDTA-plasma was obtained from the author and refrigerated at 4 °C until use. 1 mM carbamate stock solutions were prepared in MeOH. To 50 μ L of plasma, 0.5 μ L of 1 mM inhibitor were added, vortexed, and left for 30 min at room temperature. The click reaction followed a reported protocol.⁶⁴ Briefly, the samples were then diluted with 400 μ L PBS and the following reagents were added, vortexing after each addition: 2.5 μ L of 20 mM rhodamine-azide **26** in DMSO, 2.5 μ L of 200 mM TCEP in water, 42.5 μ L of 1.2 mM TBTA in *tert*-butanol, 2.5 μ L of 200 mM aqueous copper (II) sulfate, and left at room temperature. After 2 h, 5 μ L of the sample stock solution were added to 25 μ L of water and 6 μ L of the 6 \times loading buffer (125 mM Tris pH 6.8, 20% glycerol, 4% SDS, 0.005% bromophenol blue), thoroughly vortexed, and incubated for 5 min at 100 °C before loading onto the gel. Polyacrylamide gels were prepared in the following

way: 12% acrylamide separating gel (375 mM Tris pH 8.8, 0.125% SDS, 0.125% ammonium persulfate, 425 ppm TMEDA) was poured into 1.5 mm casting molds (8 mL/mold, Mini-PROTEAN[®], BioRad), covered with 1 mL of isopropanol, and left to polymerize for 25 min, then 15-well comb was inserted, covered with 5% acrylamide stacking gel (375 mM Tris pH 6.8, 0.1% SDS, 0.1% ammonium persulfate, 1000 ppm TMEDA), and left to polymerize for 25 min. 30 μ L of samples and protein standard ladder (SeeBlue[™] Plus2 Pre-stained Protein Standard, Invitrogen) was loaded onto the gel and the electrophoresis was run at 200 V for 1 h at room temperature in a cell (Mini-PROTEAN[®] Tetra, BioRad) filled with SDS-PAGE buffer (24 mM Tris, 192 mM glycine, 0.1% SDS). The proteins were then transferred onto a nitrocellulose membrane using a dry Western blot system (iBlot 2 Dry Blotting System, Thermo Fischer Scientific). Fluorescence was observed under epi green illumination (15 s exposure) and a 595 nm filter in a fluorescent imager (Uvitec Cambridge Alliance 9.7, Uvitec, Lodi, NJ, USA). For detection of hBChE, the membranes were first incubated in 5% non-fat dry milk in TTBS buffer (25 mM Tris pH 7.4, 137 mM NaCl, 3 mM KCl, 0.1% Tween 20) for 1 h at room temperature. The membranes were washed thrice with TTBS buffer for 5 min at room temperature, followed by a 1.5 h incubation at room temperature in the primary antibody solution (1:500 rabbit anti-hBChE antibody ab236577, Abcam) in 3% BSA in TTBS). The membranes were then washed thrice with TTBS buffer for 5 min at room temperature and incubated in the secondary antibody solution (1:5000 goat anti-rabbit IgG-HRP conjugate, Jackson ImmunoResearch 111-035-045 in 5% milk in TTBS) for 1 h at room temperature. The membranes were finally washed six times with TTBS buffer for 5 min at room temperature and exposed for 5 min to 700 μ L of the chemiluminescent reagent (SuperSignal[™] West Femto Maximum Sensitivity Substrate, Thermo Fisher Scientific). Chemiluminescence was observed in an imaging device (G-box, Syngene) in the dark.

Crystallization

Recombinant hBChE was produced in Chinese hamster ovary cells in a form devoid of its C-terminal end and where four residues were engineered to reduce *N*-glycosylation, as described previously.⁶⁵ Protein was purified with an initial BChE-specific affinity chromatography (Hupresin, CHEMFORASE, Rouen, France), followed by polishing and desalting with size exclusion (Superdex 200, GE Healthcare) chromatography.⁶⁶ hBChE crystals were obtained using the hanging drop method at 293 K using a 10 mg/mL protein solution and 0.1 M MES pH 6.5, 2.15 M (NH₄)₂SO₄ as crystallization buffer. Stock solution of **6** (0.1 M) was prepared in 100% MeOH and the complex with hBChE was obtained by crystal soaking in 2 mM final

ligand concentration in crystallization buffer. Crystals were cryo-protected in a solution of 0.1 M MES pH 6.5, 2.15 M (NH₄)₂SO₄, 20% glycerol, 1 mM ligand, 1% MeOH before flash cooling into liquid nitrogen.

X-ray Structure Determination

X-ray diffraction data were collected at the European Synchrotron Research Facility (ESRF; Grenoble, France) on the ID23-1 beamline at 100 K and images recorded on a Pilatus 6M detector (Dectris). Images were processed using the automatic data processing pipeline (GrenADES) based on XDS⁶⁷ for indexing, scaling, etc. Data analysis was realized using the Phenix software suite.⁶⁸ The structure of hBChE (PDB 1P0I) devoid of any ligand, glycan, or water molecules was used to determine the initial model by molecular replacement. Electron densities were observed in the active site gorge and allowed fitting of ligand. Ligand geometry restraints for the leaving group were processed using Phenix eLBOW⁶⁹ and the semi-empirical quantum mechanical method (AM1). Each model was refined by iterative cycles of Phenix.refine and model building using *Coot* (Table S1).⁷⁰ Restraints for bond formation, angles and dihedrals were applied to account for the carbamoylation of Ser198. Human BChE structure, dimethylcarbamoylated at Ser198 and in complex with **5** (leaving group of **6**), was deposited into the Protein Data Bank under accession number 8AI7.

Mass spectrometry study on whole BChE

The unglycosylated recombinant hBChE produced in *E. coli*⁶⁰ was diluted to 5 μM in MQ water, and 100 mM compound stock solutions in MeOH were further diluted with MQ water to the final concentration. The enzyme was incubated with 10 molar equivalents of the carbamate (50 μM) **6** and **14** for 5 and 20 minutes, respectively, while a non-treated aliquot served as control. Analysis was done on an Agilent 1290 Infinity UHPLC system coupled to an Agilent iFunnel Q-TOF 6550 HRMS with the following conditions: Phenomenex bioZenTM Intact XB-C8 LC 3.6 μm, 100 × 2.1 mm column, injection volume: 2 μL, mobile phase A: 0.1% HCOOH in ultrapure water, mobile phase B: 0.1% HCOOH in MeCN, flow: 0.4 mL/min, gradient elution: 0–2 min, 5% B; 2–16 min, 5%–100% B; 16–18 min, 100%B; 18–30 min; 5% B. The LC/MS data collected in the positive mode were treated using OpenChrom® software⁷¹ (v 1.4) and extracted spectra were deconvoluted with UniDec software⁷² (v 5.0.1).

Computational studies

Computational experiments were performed on workstations at the Department of Pharmaceutical Chemistry, Faculty of Pharmacy, and facilities of the Ažman Computing Centre at National Institute of Chemistry in Ljubljana, using Schrödinger Small Molecule Discovery Suite Release 2021-1 (Schrödinger, LLC, New York, USA, 2021) and Desmond/Maestro Non-commercial Distribution (Desmond v6.5, D. E. Shaw Research, New York, NY, USA, 2021).⁷³ The 6QAA and 8AI7 crystal structures were prepared using Protein Preparation Wizard: bond orders were assigned using CCD database, missing hydrogens were added, disulfide bonds were created, termini were capped, the missing side chains and loops were modelled with Prime, and het protonation states ($\text{pH } 7.0 \pm 2.0$) were modelled with Epik⁷⁴. All hets and cosolvent molecules except the co-crystallized ligands were removed. The crystal waters were retained. Hydrogen bonds were automatically assigned and optimized using PROPKA⁷⁵ ($\text{pH } 7.0$).

Noncovalent Molecular Docking

For noncovalent docking calculations, 6QAA hBChE crystal structure (resolution 1.9 Å) that was prepared as described above was used. Chain A with the co-crystallized ligand was retained while all other ligands and water molecules were removed, and Ser198 was mutated to Ala198. Receptor grid was then generated with van der Waals radii scaling by 1, partial charge cutoff was set to 0.25, and halogens were enabled as donors. The active site was defined as the centroid of the co-crystallized ligand with innerbox of 10 Å³ and outerbox of 24.076 Å³. OPLS_2005 forcefield^{76,77} was used and amide nitrogens of Gly116, Gly117, and Ala199 were defined as hydrogen donors. Ligand structures were prepared with LigPrep and ionized with Epik⁷⁴ ($\text{pH } 7 \pm 2$) using OPLS4 force field – based on the known SAR, only the structures with ionized central tertiary amine were retained. Docking was performed using Glide XP⁷⁸ with the following modifications of the default settings: intramolecular hydrogen bonds were rewarded, a constraint of at least one hydrogen bond formed as defined in the grid with an oxygen-based acceptor was introduced, and a maximum of 3 Å RMSD of the cycloheptyl ring in the docked poses (defined by C1CCCCC1) *vs.* its position in the 6QAA cognate ligand. This led to poses that had carbamate alkyls oriented towards the acyl-binding pocket (case A). Additionally, another set of noncovalent docking conditions was used (case B): intramolecular hydrogen bonds were rewarded, a constraint of at least one hydrogen bond formed as defined in the grid with an oxygen-based acceptor was introduced, and a maximum of 1 Å RMSD of the indole ring in the docked poses (defined by RMSD subset atoms) *vs.* its position in the 6QAA cognate ligand. This approach led to poses that had carbamate alkyls oriented towards the choline-binding pocket (case B). The output poses were visualized with Maestro.

Covalent Molecular Docking

The CovDock protocol⁷⁹ was used for covalent docking of the carbamate ligands. We again used the prepared 6QAA crystal structure, His438 residue was manually modified to charged HIP438 to ensure the proper postreaction structure, and Ser198 was negatively ionized. Ser198 was selected as the reactive residue, the box was defined as the centroid of the co-crystallized ligand in 6QAA with the size defined by the ligand. Reaction type was customized using a custom chemistry file (see Supporting Information) to correctly produce a negatively charged tetrahedral intermediate, since the default nucleophilic addition to a double bond led to a neutral one. No constraints were imposed and the thorough pose prediction docking mode was used. The results were visualized in Maestro and the obtained docking poses with cycloheptyl ring outside its well-defined position above Trp82 (*vide supra*) or with the ex-carbonyl anionic oxygen located outside the oxyanion hole were removed. The remaining poses were ranked by score and favourable interactions with the peripheral site residues (Tyr332, Asp70). For the case *B* poses, the prereaction poses from noncovalent docking were manually modified (bond formed between the carbonyl carbon and O γ -Ser198, and its length set to optimal, His438 protonated on N ϵ , double bond of the carbonyl changed to single, and carbonyl oxygen negatively charged) to produce the corresponding postreaction states that were later used for MD.

Molecular Dynamics

The structures from docking were used to prepare the systems for molecular dynamics (MD) simulations with System Builder. Mutated Ala198 was reverted to Ser198, and TIP4P⁸⁰ water molecules were added up to 10 Å from the protein surface to solvate the protein in a orthorhombic box. Next, Na⁺ and Cl⁻ ions were added to neutralize the system and produce the final 0.15 M concentration. OPLS_2005 force field^{76,77} was used for parametrization of the macromolecule as well as the ligand. Default Desmond relaxation protocol (desmond_npt_relax.msg) was used for the equilibration stage: (1) 100 ps of Brownian Dynamics NVT, 10 K, small timesteps, with restraints on the solute heavy atoms, (2) 12 ps NVT, 10 K, with small timesteps and restraints on the solute heavy atoms, (3) 12 ps NPT, 10 K, and restraints on the solute heavy atoms, (4) 24 ps unrestrained NPT; followed by the production stage. The following setup was used for the MD production stage: 1.2 ps interval for energy, isothermal-isobaric NPT ensemble at 300 K and 1.013 bar pressure with Langevin thermostat and barostat (1 and 2 ps relaxation time, respectively, isotropic coupling), RESPA integrator with 2 fs time step, cutoff scheme at 9.0 Å, and random seed. The simulations times were 20–1000 ns with 1000 frames per trajectory. The

simulation results were analyzed using the built-in Desmond tools. In addition, the binding pose metadynamics for the compound **6** case *A* and *B* poses obtained from noncovalent docking followed the default workflow (10 simulations/pose).

Quantum Mechanical Calculations

The quantum mechanical (QM) density functional theory (DFT) calculations for the model reaction of **6a** with methoxide were carried out in Jaguar⁸¹. After the initial rough MacroModel minimization, the structures were geometrically optimized at M06-2X/6-31G**++ level and solvent effect (water) were modelled by self-consistent reaction field method using the Poisson-Boltzmann (PBF) solver. The structures were checked for the absence of imaginary frequencies to confirm that they correspond to geometric minima. The ultrafine pseudospectral grids were used for the geometry optimization, followed by full analytic integrals for single point frequency calculation at M06-2X/cc-pVTZ(-f)++ level with PBF solver in water. For anionic intermediates, the `stop_rxn=3` and `geoconv_mode=standard` keywords had to be used to successfully model the unstable intermediates. The transition state was located utilizing the QST (quadratic synchronous transit) method and further verified by the presence of one imaginary frequency in the direction of the reaction coordinate and by an intrinsic reaction coordinate scan (IRC) in direction of both reactants and products. The calculated total energies for reactants, intermediates, and products were compared to calculate the reaction energetics.

Chemistry – General Information

The reagents and solvents were used as received from commercial suppliers. Tetrahydrofuran (THF) was distilled from sodium/benzophenone and stored under Ar over 4 Å molecular sieves prior to use. After extraction, organic phases were dried over anhydrous sodium sulfate. Reactions were monitored using analytical thin-layer chromatography (TLC) on silica gel 60 F₂₅₄ Al plates. Developed plates were inspected under UV light and, if necessary, visualized with ninhydrin, vanillin/sulfuric acid, Dragendorff's or potassium permanganate stains. Melting points were determined with Büchi 535 Melting Point Appartus (uncorrected). Nuclear magnetic resonance spectra were recorded on a Bruker Avance III 400 MHz spectrometer at 400 MHz for ¹H, 100 MHz for ¹³C, and 376 MHz for ¹⁹F nucleus, respectively, using DMSO-*d*₆ or CDCl₃ with TMS as the internal standard, as solvents. Chemical shifts are reported in *parts per million* (ppm), the central peak of the residual nondeuterated solvent signal was used as the reference, *i.e.*, for CDCl₃ at 7.27 ppm for ¹H and 77.16 ppm for ¹³C, and for DMSO-*d*₆ at 2.50 ppm for ¹H and 39.52 ppm for ¹³C. Alternatively, the TMS peak was calibrated to 0

ppm. ^{19}F spectra were not calibrated. The multiplicities are reported as follows: s (singlet), d (doublet), t (triplet), q (quartet), hept, (heptet), m (multiplet), dd (doublet of doublets), ddd (doublet doublet of doublets), td (triplet of doublets), qd (quartet of doublets), and br (broad), coupling constants (J) quoted in Hertz (Hz), number of equivalent nuclei (by integration). Mass spectra were recorded on Thermo Scientific Q Executive Plus LC-MS/MS spectrometers and IR spectra on Thermo Nicolet FT-IR spectrophotometer. Column chromatography was performed on silica gel (Silica gel 60, particle size: 0.035–0.070 mm, Merck). UPLC analyses were performed on Thermo Scientific Dionex UltiMate 3000 modular system (Thermo Fisher Scientific Inc.). The general method used a Waters Acquity UPLC[®] HSS C18 SB column (2.1 \times 50 mm, 1.8 μm) thermostated at 40 $^{\circ}\text{C}$, with: injection volume, 5 μL ; sample, 0.1–0.2 mg/mL in MeOH; flow rate, 0.4 mL/min; detector λ , 220 and 254 nm; mobile phase A: 0.1% TFA (v/v) in water; mobile phase B: MeCN. Gradient: 0–2 min, 20% B; 2–5 min, 20%–90% B; 5–8 min, 90% B. All compounds are >95% pure by UPLC analysis.

General procedure 1 (GP1) – Mannich reaction with 2-cycloheptyl-*N*-methylethan-1-amine: Parent indole (1.0 mmol) was dissolved in EtOAc (1 mL), glacial AcOH (1 mL), formaldehyde (1.2 eq., 37%, 89 μL), and 2-cycloheptyl-*N*-methylethan-1-amine⁸² (171 mg, 1.1 eq.) were added, and the reaction mixture was stirred at rt for 18 h. The volatile components were removed *in vacuo* and the product was purified following GP2.

General procedure 2 (GP2) – RP-CC purification: Compounds were purified by reversed-phase column chromatography (RP-CC) (Isolera Biotage One Flash Chromatography system, Biotage[®] Sfär C18 Duo 100 Å 30 μm column, 30 g) using a gradient of 0.1% TFA in deionized water and MeCN as eluent (gradient 0–100% MeCN in 6 column volumes (300 mL); 100% MeCN for 2 column volumes (100 mL)). After the RP-CC, fractions containing the product were combined and organic volatiles were evaporated *in vacuo*. The remaining aqueous solution was made alkaline (pH 10) with 1 M NaOH_(aq) and extracted with DCM (2 \times 30 mL). The combined organic phase was dried over anhydrous sodium sulfate, filtered, and volatile components evaporated *in vacuo* to afford pure product.

3-(((2-Cycloheptylethyl)(methyl)amino)methyl)-1*H*-indol-7-ol (5)

1*H*-Indol-7-ol⁸³ (92 mg, 0.692 mmol), TBDMSCl (1.1 eq., 114 mg), and imidazole (1.2 eq., 56 mg) in DMF (2 mL) were stirred at rt under Ar for 18 h. 7-(((*Tert*-butyldimethylsilyl)oxy)-1*H*-indole⁸⁴ was isolated by column chromatography on silica (1. PE; 2. PE/DCM = 5:1). Yield: 138 mg (0.558 mmol, 80.6%). *N*-((7-(((*Tert*-butyldimethylsilyl)oxy)-1*H*-indol-3-yl)methyl)-2-cycloheptyl-*N*-methylethan-1-amine was prepared following GP1 from 7-((*tert*-

butyldimethylsilyl)oxy)-1*H*-indole (124 mg, 0.5 mmol), and isolated by *GP2*. Yield: 156 mg (0.376 mmol, 75.2%) of beige semisolid. ESI-HRMS: $m/z = 415.3128$ (MH^+); $C_{25}H_{43}N_2OSi$ requires: $m/z = 415.3139$ (MH^+). ν_{max} 3490, 2924, 2854, 2787, 1622, 1577, 1498, 1461, 1360, 1337, 1253, 1078, 994, 833, 781, 729, 681 cm^{-1} . 1H NMR (400 MHz, $CDCl_3$) $\delta = 0.27$ (s, 6H), 1.05 (s, 9H), 1.13 – 1.21 (m, 2H), 1.34 – 1.70 (m, 13H), 2.23 (s, 3H), 2.42 – 2.46 (m, 2H), 3.68 (s, 2H), 6.62 (d, $J=7.4$, 1H), 6.96 (t, $J=7.8$, 1H), 7.11 (d, $J=2.0$, 1H), 7.29 – 7.31 (m, 1H), 8.05 (s, 1H). ^{13}C NMR (101 MHz, $CDCl_3$) $\delta = -4.09$, 18.37, 25.95, 26.57, 28.61, 34.90, 35.90, 37.68, 42.47, 52.97, 55.86, 110.15, 112.74, 114.17, 119.92, 123.07, 129.36, 130.05, 141.42.

N-(((7-((*Tert*-butyldimethylsilyl)oxy)-1*H*-indol-3-yl)methyl)-2-cycloheptyl-*N*-methylethan-1-amine (100 mg, 0.241 mmol) and potassium bifluoride (20 eq., 376 mg) in MeOH (5 mL) were stirred at rt under Ar for 6 h. 3-(((2-Cycloheptylethyl)(methyl)amino)methyl)-1*H*-indol-7-ol was isolated following *GP2*. Yield: 42 mg (0.14 mmol, 58.0%) of brownish semisolid, unstable in air. ESI-HRMS: $m/z = 301.2261$ (MH^+); $C_{19}H_{29}N_2O$ requires: $m/z = 301.2274$ (MH^+). ν_{max} 2919, 2850, 1673, 1577, 1442, 1361, 1249, 1099, 1050, 976, 787, 728 cm^{-1} . Purity: UPLC (220 nm): $t_r = 4.150$ min, 99.2% total area. 1H NMR (400 MHz, $CDCl_3$) $\delta = 1.00 - 1.09$ (m, 2H), 1.24 – 1.56 (m, 14H), 2.26 (s, 3H), 2.54 – 2.61 (m, 2H), 3.80 (s, 2H), 6.59 (d, $J=7.3$, 1H), 6.89 – 6.97 (m, 2H), 7.01 (d, $J=7.9$, 1H), 9.81 (br s, 1H), 10.36 (br s, 1H). ^{13}C NMR (101 MHz, $CDCl_3$) $\delta = 26.36$, 28.51, 34.12, 34.59, 37.75, 40.72, 52.06, 55.40, 107.92, 108.73, 109.01, 120.96, 125.12, 128.11, 129.87, 145.58.

3-(((2-Cycloheptylethyl)(methyl)amino)methyl)-1*H*-indol-7-yl dimethylcarbamate (6)

7-(Benzyloxy)-1*H*-indole (500 mg, 2.24 mmol) was dissolved in EtOAc (15 mL), flushed with Ar, then 10% Pd/C (50 mg) was added, and the resulting mixture was hydrogenated at rt under H_2 (balloon pressure) for 24 h. The catalyst was removed by filtration, washed with EtOAc (10 mL), and the filtrate evaporated *in vacuo* to afford crude 1*H*-indol-7-ol as grayish semisolid, unstable in air. Yield: 292 mg (2.19 mmol, 97.8%).

1*H*-Indol-7-ol (150 mg, 1.13 mmol), *N,N*-dimethylcarbamoyl chloride (1.5 eq., 156 μ L), and DIPEA (500 μ L) in MeCN (3 mL) were stirred at rt under Ar for 18 h. 1*H*-Indol-7-yl dimethylcarbamate⁸⁵ was isolated by column chromatography on silica (1. PE/EtOAc = 4:1; 2. PE/EtOAc = 1:1). Yield: 69 mg (0.338 mmol, 29.9%) of beige semisolid.

[Note: the C3-carbamoylation seems to be a competing reaction. The *O*-carbamoylated product turns red, not blue, upon spraying and heating the TLC plate with

vanillin/sulfuric acid. The selective *O*-carbamoylation can be achieved by substituting DIPEA for *N*-methylimidazole – carbamoyl chloride and *N*-methylimidazole are premixed for 5 min, then indolol is added, and the mixture stirred at 80 °C for 6 h.]

ESI-HRMS: $m/z = 205.0968$ (MH^+); $C_{11}H_{13}N_2O_2$ requires: $m/z = 205.0972$ (MH^+). ν_{max} 3276, 2924, 1699, 1496, 1445, 1392, 1342, 1232, 1217, 1173, 1044, 847, 783, 722 cm^{-1} . Purity: UPLC (220 nm): $t_r = 3.803$ min, 95.2% total area. 1H NMR (400 MHz, $CDCl_3$) $\delta = 3.06$ (s, 3H), 3.17 (s, 3H), 6.56 (dd, $J=2.1, 3.2$, 1H), 6.96 – 6.99 (m, 1H), 7.06 – 7.10 (m, 1H), 7.12 (t, $J=2.7$, 1H), 7.48 – 7.52 (m, 1H), 8.56 (br s, 1H). ^{13}C NMR (101 MHz, $CDCl_3$) $\delta = 36.75, 103.09, 113.78, 117.96, 119.80, 124.83, 128.57, 130.97, 137.17, 154.59$.

3-(((2-Cycloheptylethyl)(methyl)amino)methyl)-1*H*-indol-7-yl dimethylcarbamate was prepared following *GPI* from 1*H*-indol-7-yl dimethylcarbamate (36 mg, 0.176 mmol). Yield: 25 mg (0.0673 mmol, 38.2%) of beige semisolid. ESI-HRMS: $m/z = 372.2640$ (MH^+); $C_{22}H_{34}N_3O_2$ requires: $m/z = 372.2646$ (MH^+). ν_{max} 3298, 2917, 2850, 2784, 1714, 1699, 1449, 1394, 1349, 1224, 1174, 1048, 1026, 846, 784, 755, 734 cm^{-1} . Purity: UPLC (220 nm): $t_r = 4.453$ min, 99.7% total area. 1H NMR (400 MHz, $CDCl_3$) $\delta = 1.13 - 1.22$ (m, 2H), 1.35 – 1.71 (m, 13H), 2.21 (s, 3H), 2.39 – 2.44 (m, 2H), 3.05 (s, 3H), 3.17 (s, 3H), 3.67 (s, 2H), 6.94 (dd, $J=0.7, 7.7$, 1H), 7.03 – 7.09 (m, 2H), 7.53 – 7.56 (m, 1H), 8.38 (s, 1H). ^{13}C NMR (101 MHz, $CDCl_3$) $\delta = 26.58, 28.62, 34.92, 35.88, 36.81, 36.98, 37.73, 42.40, 52.91, 55.86, 113.86, 114.09, 116.85, 119.56, 124.12, 128.98, 131.15, 137.09, 154.56$.

3-(((2-Cycloheptylethyl)(methyl)amino)methyl)-1*H*-indol-7-yl ethyl(methyl)carbamate (7)

1*H*-Indol-7-ol (181 mg, 1.36 mmol), ethylmethylcarbamoyl chloride (1.5 eq., 248 mg), and DIPEA (500 μ L) in MeCN (3 mL) were stirred at rt under Ar for 18 h. 1*H*-Indol-7-yl ethyl(methyl)carbamate was isolated by column chromatography on silica (PE/EtOAc = 4:1). Yield: 102 mg (0.467 mmol, 34.4%) of beige semisolid, that was immediately used further.

3-(((2-Cycloheptylethyl)(methyl)amino)methyl)-1*H*-indol-7-yl ethyl(methyl)carbamate was prepared following *GPI* from 1*H*-indol-7-yl ethyl(methyl)carbamate (75 mg, 0.344 mmol). Yield: 65 mg (0.169 mmol, 49.0%) of brown oil. ESI-HRMS: $m/z = 386.2796$ (MH^+); $C_{23}H_{36}N_3O_2$ requires: $m/z = 386.2802$ (MH^+). ν_{max} 3307, 2918, 2851, 2788, 1703, 1445, 1399, 1349, 1301, 1286, 1222, 1164, 1088, 971, 783, 756, 730 cm^{-1} . Purity: UPLC (254 nm): $t_r = 4.533$ min, 98.6% total area.

3-(((2-Cycloheptylethyl)(methyl)amino)methyl)-1*H*-indol-7-yl isopropyl(methyl)carbamate (8)

N-Isopropylmethylamine (500 μ L, 4.8 mmol) and CDI (1.0 eq., 778 mg) in DCM (5 mL) were stirred at rt for 12 h. The reaction mixture was extracted with water (10 mL, discarded), dried with sodium sulfate, the solvent was removed *in vacuo*, the residue dissolved in MeCN (5 mL), iodomethane (1.2 eq., 448 μ L) was added, and the mixture stirred under Ar at rt for 18 h. The solvent was removed *in vacuo*, the residue redissolved in MeCN (5 mL), 1*H*-indol-7-ol (141 mg, 1.06 mmol) and DIPEA (500 μ L) were added, and the reaction mixture stirred at 60 °C for 4 h. The solvent was removed *in vacuo* and 1*H*-indol-7-yl isopropyl(methyl)carbamate isolated by column chromatography on silica (PE/EtOAc = 4:1). Yield: 193 mg (0.831 mmol, 78.4%) of pinkish solid. mp 86.5–87.2 °C. ESI-HRMS: m/z = 233.1296 (MH^+); $C_{13}H_{17}N_2O_2$ requires: m/z = 233.1285 (MH^+). ν_{max} 3317, 2981, 1686, 1495, 1437, 1397, 1335, 1229, 1214, 1119, 889, 777, 724 cm^{-1} . Purity: UPLC (254 nm): t_r = 4.647 min, 99.7% total area. 1H NMR (400 MHz, $CDCl_3$) δ = 1.21 – 1.33 (m, 6H), 2.94 and 3.01 (2 x s, 3H), 4.52 – 4.68 (m, 1H), 6.57 (dd, J =2.1, 3.1, 1H), 6.99 (t, J =8.4, 1H), 7.10 (t, J =7.8, 1H), 7.11 – 7.17 (m, 1H), 7.51 (d, J =7.8, 1H), 8.47 – 8.61 (m, 1H). ^{13}C NMR (101 MHz, $CDCl_3$) δ = 19.67, 20.28, 27.84, 27.92, 47.30, 47.74, 103.06, 113.68, 117.86, 119.77, 124.77, 130.93, 137.23, 153.95. Carbamate carbons are duplicated due to two rotamer populations.

3-(((2-Cycloheptylethyl)(methyl)amino)methyl)-1*H*-indol-7-yl isopropyl(methyl)carbamate was prepared following *GPI* from 1*H*-indol-7-yl isopropyl(methyl)carbamate (133 mg, 0.573 mmol). Yield: 139 mg (0.348 mmol, 60.7%) of beige oil. ESI-HRMS: m/z = 400.2952 (MH^+); $C_{24}H_{38}N_3O_2$ requires: m/z = 400.2959 (MH^+). ν_{max} 3319, 2920, 2851, 2790, 1698, 1499, 1444, 1334, 1223, 1170, 1121, 1004, 908, 822, 755, 730 cm^{-1} . Purity: UPLC (254 nm): t_r = 4.647 min, 99.7% total area. 1H NMR (400 MHz, $CDCl_3$) δ = 1.17 – 1.28 (m, 8H), 1.16 – 1.29 (m, 1H), 1.37 – 1.74 (m, 13H), 2.22 (s, 3H), 2.41 – 2.46 (m, 2H), 2.91 and 2.98 (2 x s, 3H), 3.68 (s, 2H), 4.49 – 4.64 (m, 1H), 6.95 (t, J =8.3, 1H), 7.04 (d, J =2.2, 1H), 7.07 (t, J =7.8, 1H), 7.56 (d, J =7.9, 1H), 8.56 and 8.63 (2 x s, 1H). ^{13}C NMR (101 MHz, $CDCl_3$) δ = 19.59, 20.21, 26.45, 27.75, 27.80, 28.49, 34.79, 35.74, 37.60, 42.22, 47.19, 47.62, 52.77, 55.71, 113.62, 113.70, 116.53, 116.61, 119.34, 124.12, 128.92, 131.02, 137.05, 153.93, 154.08. Two sets of rotamer signals.

3-(((2-Cycloheptylethyl)(methyl)amino)methyl)-1*H*-indol-7-yl *tert*-butyl(methyl)carbamate (9)

N-Methyl-*tert*-butylamine (200 μ L, 1.67 mmol) and CDI (1.0 eq., 271 mg) in DCM (5 mL) were stirred at rt for 12 h. The reaction mixture was extracted with water (10 mL, discarded), dried with sodium sulfate, the solvent was removed *in vacuo*, the residue dissolved in MeCN (5 mL), iodomethane (1.2 eq., 156 μ L) was added, and the mixture stirred under Ar at rt for 18 h. The solvent was removed *in vacuo*, the residue redissolved in MeCN (5 mL), 1*H*-indol-7-ol (97 mg, 0.73 mmol) and DIPEA (500 μ L) were added, and the reaction mixture stirred at 60 °C for 4 h. The solvent was removed *in vacuo* and 1*H*-indol-7-yl *tert*-butyl(methyl)carbamate isolated by column chromatography on silica (PE/EtOAc = 4:1). Yield: 130 mg (0.528 mmol, 72.3%) of beige semisolid [¹H NMR (400 MHz, CDCl₃) δ = 1.55 (s, 9H), 3.17 (s, 3H), 6.59 (dd, *J*=2.1, 3.2, 1H), 7.00 (dd, *J*=0.7, 7.7, 1H), 7.11 (t, *J*=7.8, 1H), 7.14 – 7.16 (m, 1H), 7.50 – 7.53 (m, 1H), 8.46 (s, 1H). ¹³C NMR (101 MHz, CDCl₃) δ = 28.67, 32.00, 56.40, 103.06, 113.83, 117.70, 119.77, 124.73, 128.72, 130.85, 137.08, 154.10.], that was immediately used further following *GPI* to afford 3-(((2-cycloheptylethyl)(methyl)amino)methyl)-1*H*-indol-7-yl *tert*-butyl(methyl)carbamate. Yield: 156 mg (0.377 mmol, 71.4%) of beige oil. ESI-HRMS: *m/z* = 414.3104 (MH⁺); C₂₅H₄₀N₃O₂ requires: *m/z* = 414.3115 (MH⁺). ν_{max} 3352, 2919, 2851, 2789, 1705, 1632, 1579, 1458, 1345, 1221, 1157, 1110, 995, 842, 757, 730 cm⁻¹. Purity: UPLC (220 nm): *t_r* = 4.783 min, 99.4% total area. ¹H NMR (400 MHz, CDCl₃) δ = 1.16 – 1.25 (m, 2H), 1.36 – 1.75 (m, 22H), 2.23 (s, 3H), 2.42 – 2.47 (m, 2H), 3.14 (s, 3H), 3.69 (s, 2H), 6.95 (dd, *J*=0.7, 7.7, 1H), 7.03 – 7.10 (m, 2H), 7.56 (d, *J*=7.9, 1H), 8.45 (s, 1H). ¹³C NMR (101 MHz, CDCl₃) δ = 26.48, 28.52, 28.65, 31.97, 34.82, 35.78, 37.62, 42.24, 52.81, 55.72, 56.34, 113.82, 116.54, 119.41, 124.04, 129.09, 131.01, 136.94, 154.09.

3-(((2-Cycloheptylethyl)(methyl)amino)methyl)-1*H*-indol-7-yl benzyl(methyl)carbamate (10)

N-Methylbenzylamine (200 μ L, 1.55 mmol) and CDI (1.0 eq., 251 mg) in DCM (5 mL) were stirred at rt for 12 h. The reaction mixture was extracted with water (10 mL, discarded), dried with sodium sulfate, the solvent was removed *in vacuo*, the residue dissolved in MeCN (5 mL), iodomethane (1.2 eq., 145 μ L) was added, and the mixture stirred under Ar at rt for 18 h. The solvent was removed *in vacuo*, the residue redissolved in MeCN (5 mL), 1*H*-indol-7-ol (97 mg, 0.73 mmol) and DIPEA (500 μ L) were added, and the reaction mixture stirred at 60 °C for 4 h. The solvent was removed *in vacuo* and 1*H*-indol-7-yl benzyl(methyl)carbamate isolated by column chromatography on silica (PE/EtOAc = 4:1). Yield: 168 mg (0.599 mmol, 82.1%) of beige semisolid, that was immediately used further following *GPI* to afford 3-(((2-cycloheptylethyl)(methyl)amino)methyl)-1*H*-indol-7-yl benzyl(methyl)carbamate. Yield: 221

mg (0.494 mmol, 82.4%) of beige oil. ESI-HRMS: m/z = 448.2951 (MH^+); $C_{28}H_{38}N_3O_2$ requires: m/z = 448.2959 (MH^+). ν_{max} 3323, 2919, 2851, 2783, 1704, 1633, 1580, 1452, 1397, 1351, 1216, 1168, 1125, 1028, 730, 698 cm^{-1} . Purity: UPLC (220 nm): t_r = 4.820 min, 99.4% total area. 1H NMR (400 MHz, $CDCl_3$) δ = 1.19 – 1.29 (m, 2H), 1.41 – 1.78 (m, 13H), 2.24 and 2.26 (2 x s, 3H), 2.44 – 2.52 (m, 2H), 3.08 and 3.10 (2 x s, 3H), 3.70 and 3.73 (2 x s, 2H), 4.58 and 4.66 (2 x s, 2H), 6.93 – 7.16 (m, 3H), 7.34 – 7.48 (m, 5H), 7.55 – 7.65 (m, 1H), 8.13 and 8.80 (2 x s, 1H). ^{13}C NMR (101 MHz, $CDCl_3$) δ = 26.42, 28.46, 34.21, 34.75, 35.55, 35.68, 37.55, 42.15, 52.71, 52.87, 53.13, 55.69, 113.61, 113.67, 113.86, 116.68, 119.27, 124.02, 124.23, 127.09, 127.62, 128.01, 128.66, 128.75, 128.86, 130.82, 131.03, 136.68, 136.86, 136.97, 137.61, 154.27, 154.77. Two rotamers in a 56:44 ratio.

3-(((2-Cycloheptylethyl)(methyl)amino)methyl)-1H-indol-7-yl diethylcarbamate (11)

1H-Indol-7-ol (128 mg, 0.961 mmol), *N,N*-diethylcarbamoyl chloride (1.1 eq., 143 mg), and caesium carbonate (1.0 eq., 313 mg) in THF (3 mL) were stirred at rt under Ar for 18 h. 1H-Indol-7-yl diethylcarbamate was isolated by column chromatography on silica (1. PE/EtOAc = 10:1; 2. PE/EtOAc = 3:1). Yield: 48 mg (0.207 mmol, 21.5%) of beige semisolid that was immediately used further following *GPI* to prepare 3-(((2-cycloheptylethyl)(methyl)amino)methyl)-1H-indol-7-yl diethylcarbamate. Yield: 53 mg (0.133 mmol, 66.0%) of beige semisolid. ESI-HRMS: m/z = 400.2949 (MH^+); $C_{24}H_{38}N_3O_2$ requires: m/z = 400.2959 (MH^+). ν_{max} 3323, 2973, 2919, 2851, 2787, 1700, 1474, 1457, 1417, 1348, 1273, 1218, 1156, 1096, 982, 757, 730 cm^{-1} . 1H NMR (400 MHz, $CDCl_3$) δ = 1.14 – 1.73 (m, 21H), 2.21 (s, 3H), 2.40 – 2.45 (m, 2H), 3.43 (q, J =7.0, 2H), 3.51 (q, J =6.9, 2H), 3.68 (s, 2H), 6.95 (dd, J =0.7, 7.7, 1H), 7.04 – 7.09 (m, 2H), 7.55 (d, J =7.9, 1H), 8.44 (s, 1H). ^{13}C NMR (101 MHz, $CDCl_3$) δ = 13.51, 14.45, 26.56, 28.60, 34.90, 35.86, 37.72, 42.28, 42.36, 42.53, 52.87, 55.82, 113.72, 114.01, 116.72, 119.51, 124.15, 129.01, 131.17, 137.13, 153.89.

3-(((2-Cycloheptylethyl)(methyl)amino)methyl)-1H-indol-7-yl diisopropylcarbamate (12)

1H-Indol-7-ol (95 mg, 0.713 mmol), *N,N*-diisopropylcarbamoyl chloride (1.5 eq., 175 mg), and DIPEA (500 μ L) in MeCN (3 mL) were stirred at rt under Ar for 18 h. 1H-Indol-7-yl diisopropylcarbamate was isolated by column chromatography on silica (PE/EtOAc = 4:1). Yield: 51 mg (0.196 mmol, 27.5%) of beige solid. mp 92.8–95.1 °C. ESI-HRMS: m/z = 261.1594 (MH^+); $C_{15}H_{21}N_2O_2$ requires: m/z = 261.1598 (MH^+). ν_{max} 3514, 3459, 3177, 2976, 2964, 2933, 1655, 1433, 1310, 1221, 1204, 1149, 1122, 1055, 1041, 897, 774, 717 cm^{-1} . 1H NMR (400 MHz, $CDCl_3$) δ = 1.35 (br s, 6H), 1.41 (br s, 6H), 4.03 (br s, 1H), 4.19 (br s, 1H),

6.58 (dd, $J=2.1, 3.2$, 1H), 6.97 (dd, $J=0.7, 7.7$, 1H), 7.08 (t, $J=7.8$, 1H), 7.19 – 7.21 (m, 1H), 7.48 – 7.50 (m, 1H), 8.46 (s, 1H). ^{13}C NMR (101 MHz, CDCl_3) δ = 20.59, 21.84, 46.37, 47.30, 103.27, 113.73, 117.81, 119.90, 124.81, 128.80, 131.04, 137.17, 153.53.

3-(((2-Cycloheptylethyl)(methyl)amino)methyl)-1*H*-indol-7-yl diisopropylcarbamate was prepared following *GPI* from 1*H*-indol-7-yl diisopropylcarbamate (31 mg, 0.119 mmol). Yield: 13 mg (0.0304 mmol, 25.5%) of light brownish oil. ESI-HRMS: m/z = 428.3267 (MH^+); $\text{C}_{26}\text{H}_{42}\text{N}_3\text{O}_2$ requires: m/z = 428.3272 (MH^+). ν_{max} 3367, 2969, 2919, 2851, 2784, 1696, 1434, 1295, 1223, 1208, 1151, 1042, 1009, 823, 757, 730 cm^{-1} . Purity: UPLC (220 nm): t_r = 4.937 min, 98.7% total area. ^1H NMR (400 MHz, CDCl_3) δ = 1.10 – 1.73 (m, 27H), 2.21 (s, 3H), 2.40 – 2.44 (m, 2H), 3.68 (s, 2H), 4.01 (br s, 1H), 4.17 (br s, 1H), 6.94 (dd, $J=0.6, 7.5$, 1H), 7.06 (t, $J=7.8$, 1H), 7.11 (d, $J=2.2$, 1H), 7.54 (d, $J=7.9$, 1H), 8.31 (s, 1H). ^{13}C NMR (101 MHz, CDCl_3) δ = 20.60, 21.84, 26.60, 28.63, 34.94, 35.91, 37.76, 42.41, 46.34, 47.29, 52.92, 55.84, 113.78, 114.14, 116.69, 119.60, 124.12, 129.20, 131.20, 137.05, 153.56.

3-(((2-Cycloheptylethyl)(methyl)amino)methyl)-1*H*-indol-7-yl piperidine-1-carboxylate (13)

1*H*-Indol-7-ol (117 mg, 0.879 mmol), piperidine-1-carbonyl chloride (1.1 eq., 143 mg), and caesium carbonate (1.0 eq., 286 mg) in THF (3 mL) were stirred at rt under Ar for 18 h. 1*H*-Indol-7-yl piperidine-1-carboxylate was isolated by column chromatography on silica (1. PE/EtOAc = 10:1; 2. PE/EtOAc = 3:1, yield: 174 mg, 0.712 mmol, 81.0%), and immediately used further following *GPI* to prepare 3-(((2-cycloheptylethyl)(methyl)amino)methyl)-1*H*-indol-7-yl piperidine-1-carboxylate. Yield: 98 mg (0.238 mmol, 47.6%) of brownish semisolid. ESI-HRMS: m/z = 412.2948 (MH^+); $\text{C}_{25}\text{H}_{38}\text{N}_3\text{O}_2$ requires: m/z = 412.2959 (MH^+). ν_{max} 3324, 2920, 2852, 2791, 1700, 1421, 1348, 1218, 1141, 1021, 953, 728 cm^{-1} . Purity: UPLC (254 nm): t_r = 4.667 min, 99.8% total area. ^1H NMR (400 MHz, CDCl_3) δ = 1.14 – 1.23 (m, 2H), 1.35 – 1.72 (m, 19H), 2.21 (s, 3H), 2.39 – 2.45 (m, 2H), 3.54 (br s, 2H), 3.64 – 3.72 (m, 4H), 6.94 (dd, $J=0.7, 7.7$, 1H), 7.04 – 7.09 (m, 2H), 7.54 (d, $J=7.6$, 1H), 8.51 (s, 1H). ^{13}C NMR (101 MHz, CDCl_3) δ = 24.32, 25.58, 26.01, 26.52, 28.56, 34.86, 35.79, 37.69, 42.30, 45.30, 45.82, 52.81, 55.79, 113.77, 113.83, 116.66, 119.46, 124.15, 129.00, 131.06, 137.07, 153.36.

3-(((2-Cycloheptylethyl)(methyl)amino)methyl)-1*H*-indol-7-yl morpholine-4-carboxylate (14)

1*H*-Indol-7-ol (100 mg, 0.751 mmol), morpholine-4-carbonyl chloride (1.5 eq., 169 mg), and DIPEA (500 μL) in MeCN (3 mL) were stirred at rt under Ar for 18 h. 1*H*-Indol-7-yl

morpholine-4-carboxylate was isolated by column chromatography on silica (1. PE/EtOAc = 5:1; 2. PE/EtOAc = 2:1). Yield: 106 mg (0.430 mmol, 57.3%) of beige solid. mp 151.2–152.5 °C. ESI-HRMS: m/z = 247.1074 (MH^+); $\text{C}_{13}\text{H}_{15}\text{N}_2\text{O}_3$ requires: m/z = 247.1077 (MH^+). ν_{max} 3332, 3295, 2989, 2957, 2919, 2865, 1693, 1412, 1342, 1230, 1210, 1113, 1082, 978, 855, 779, 720 cm^{-1} . ^1H NMR (400 MHz, CDCl_3) δ = 3.59 – 3.65 (m, 2H), 3.73 – 3.79 (m, 6H), 6.58 (dd, J =2.0, 3.1, 1H), 6.96 (d, J =7.7, 1H), 7.08 (t, J =7.8, 1H), 7.17 (t, J =2.6, 1H), 7.51 (d, J =7.9, 1H), 8.46 (s, 1H). ^{13}C NMR (101 MHz, CDCl_3) δ = 44.37, 45.17, 66.59, 66.72, 103.31, 113.78, 118.26, 119.89, 124.85, 128.45, 131.08, 136.87, 153.36.

3-(((2-Cycloheptylethyl)(methyl)amino)methyl)-1*H*-indol-7-yl morpholine-4-carboxylate was prepared following *GPI* from 1*H*-indol-7-yl morpholine-4-carboxylate (69 mg, 0.280 mmol). Yield: 36 mg (0.087 mmol, 31.1%) of beige solid. mp 111.2–112.9 °C. ESI-HRMS: m/z = 414.2744 (MH^+); $\text{C}_{24}\text{H}_{36}\text{N}_3\text{O}_3$ requires: m/z = 414.2751 (MH^+). ν_{max} 3327, 2917, 2857, 2797, 2767, 1699, 1452, 1417, 1352, 1245, 1220, 1162, 1119, 1101, 854, 782, 754, 736, 624 cm^{-1} . Purity: UPLC (220 nm): t_r = 4.113 min, 99.9% total area. ^1H NMR (400 MHz, CDCl_3) δ = 1.13 – 1.22 (m, 2H), 1.34 – 1.71 (m, 13H), 2.21 (s, 3H), 2.40 – 2.44 (m, 2H), 3.61 (br s, 2H), 3.67 (s, 2H), 3.73 – 3.80 (m, 6H), 6.93 (d, J =7.1, 1H), 7.07 (t, J =7.8, 1H), 7.09 (d, J =2.2, 1H), 7.57 (d, J =7.9, 1H), 8.34 (s, 1H). ^{13}C NMR (101 MHz, CDCl_3) δ = 26.58, 28.62, 34.92, 35.90, 37.71, 42.44, 44.37, 45.18, 52.96, 55.90, 66.62, 66.76, 113.84, 114.37, 117.16, 119.60, 124.11, 128.86, 131.23, 136.77, 153.38.

3-(((2-Cycloheptylethyl)(methyl)amino)methyl)-1*H*-indol-7-yl methyl(prop-2-yn-1-yl)carbamate (15)

N-Methylpropargylamine (150 μL , 1.78 mmol) and CDI (1.0 eq., 289 mg) in DCM (5 mL) were stirred at rt for 12 h. The reaction mixture was extracted with water (10 mL, discarded), dried with sodium sulfate, the solvent was removed *in vacuo*, the residue dissolved in MeCN (5 mL), iodomethane (1.2 eq., 166 μL) was added, and the mixture stirred under Ar at rt for 18 h. The solvent was removed *in vacuo*, the residue redissolved in MeCN (5 mL), 1*H*-indol-7-ol (97 mg, 0.73 mmol) and DIPEA (500 μL) were added, and the reaction mixture stirred at 60 °C for 4 h. The solvent was removed *in vacuo* and 1*H*-indol-7-yl methyl(prop-2-yn-1-yl)carbamate isolated by column chromatography on silica (PE/EtOAc = 4:1). Yield: 119 mg (0.521 mmol, 82.1%) of beige semisolid, that was immediately used further following *GPI* to afford 3-(((2-cycloheptylethyl)(methyl)amino)methyl)-1*H*-indol-7-yl methyl(prop-2-yn-1-yl)carbamate. Yield: 111 mg (0.281 mmol, 53.9%) of beige oil. ESI-HRMS: m/z = 396.2640 (MH^+); $\text{C}_{24}\text{H}_{34}\text{N}_3\text{O}_2$ requires: m/z = 396.2646 (MH^+). ν_{max} 3306, 2919, 2850, 2788, 1706, 1634, 1580,

1443, 1394, 1348, 1218, 1167, 1138, 1031, 787, 731, 657 cm⁻¹. Purity: UPLC (220 nm): *t_r* = 4.527 min, 99.9% total area. ¹H NMR (400 MHz, CDCl₃) δ = 1.14 – 1.24 (m, 2H), 1.35 – 1.74 (m, 13H), 2.21 (s, 3H), 2.32 – 2.46 (m, 3H), 3.09 and 3.20 (2 x s, 3H), 3.68 (s, 2H), 4.23 and 4.26 (2 x s, 2H), 6.95 – 7.04 (m, 2H), 7.07 (t, *J*=7.6, 1H), 7.57 (d, *J*=7.8, 1H), 8.56 and 8.60 (2 x s, 1H). ¹³C NMR (101 MHz, CDCl₃) δ = 26.49, 28.53, 33.94, 34.65, 34.82, 35.78, 37.61, 38.59, 39.02, 42.27, 52.82, 55.77, 72.65, 72.82, 78.30, 78.92, 113.74, 113.98, 117.00, 119.37, 124.07, 124.20, 128.70, 128.82, 130.95, 131.11, 136.59, 136.78, 153.77, 154.11. Two sets of conformers.

3-(((2-Cycloheptylethyl)(methyl)amino)methyl)-1*H*-indol-7-yl methyl(pent-4-yn-1-yl)carbamate (16)

N-Methylpent-4-yn-1-amine⁸⁶ (486 mg, 5.0 mmol) and CDI (1.0 eq., 811 mg) in DCM (5 mL) were stirred at rt for 12 h. The reaction mixture was extracted with water (10 mL, discarded), dried with sodium sulfate, the solvent was removed *in vacuo*, the residue dissolved in MeCN (5 mL), iodomethane (1.2 eq., 374 μL) was added, and the mixture stirred under Ar at rt for 18 h. The solvent was removed *in vacuo*, the residue redissolved in MeCN (5 mL), 1*H*-indol-7-ol (157 mg, 1.18 mmol) and DIPEA (500 μL) were added, and the reaction mixture stirred at 60 °C for 4 h. The solvent was removed *in vacuo* and 1*H*-indol-7-yl methyl(pent-4-yn-1-yl)carbamate isolated by column chromatography on silica (PE/EtOAc = 4:1). Yield: 254 mg (0.991 mmol, 84.0%) of beige oil. ESI-HRMS: *m/z* = 257.1280 (MH⁺); C₁₅H₁₇N₂O₂ requires: *m/z* = 257.1285 (MH⁺). *v*_{max} 3292, 2936, 1698, 1398, 1341, 1232, 1186, 1127, 1053, 786, 723, 636 cm⁻¹. ¹H NMR (400 MHz, CDCl₃) δ = 1.90 (dp, *J*=6.9, 14.1, 2H), 2.09 and 2.11 (t, *J*=2.6, 1H), 2.30 – 2.39 (m, 2H), 3.05 and 3.15 (2 x s, 3H), 3.51 (t, *J*=7.0, 1H), 3.63 (t, *J*=6.9, 1H), 6.56 – 6.59 (m, 1H), 7.02 (t, *J*=7.9, 1H), 7.07 – 7.14 (m, 2H), 7.52 (d, *J*=7.8, 1H), 8.67 and 8.73 (2 x s, 1H). ¹³C NMR (101 MHz, CDCl₃) δ = 15.87, 15.99, 26.13, 26.63, 34.92, 34.95, 48.31, 48.68, 69.00, 69.40, 83.70, 83.77, 102.89, 102.93, 113.63, 117.82, 119.66, 124.72, 124.76, 128.42, 128.48, 130.80, 130.84, 137.04, 154.27, 154.32. Two sets of conformer signals.

3-(((2-Cycloheptylethyl)(methyl)amino)methyl)-1*H*-indol-7-yl methyl(pent-4-yn-1-yl)carbamate was prepared following *GPI* from 1*H*-indol-7-yl methyl(pent-4-yn-1-yl)carbamate (99 mg, 0.387 mmol). Yield: 103 mg (0.243 mmol, 38.2%) of beige oil. ESI-HRMS: *m/z* = 424.2951 (MH⁺); C₂₆H₃₈N₃O₂ requires: *m/z* = 424.2959 (MH⁺). *v*_{max} 3309, 2920, 2851, 2789, 1705, 1444, 1399, 1349, 1303, 1223, 1187, 1127, 731, 632 cm⁻¹. Purity: UPLC (254 nm): *t_r* = 4.717 min, 97.5% total area. ¹H NMR (400 MHz, CDCl₃) δ = 1.14 – 1.24 (m, 2H), 1.36 – 1.72 (m, 13H), 1.89 (dp, *J*=6.9, 20.8, 2H), 2.03 and 2.07 (t, *J*=2.5, 1H), 2.21 (s, 3H), 2.30 (td, *J*=2.6, 6.9, 1H), 2.34 (td, *J*=2.6, 6.7, 1H), 2.40 – 2.45 (m, 2H), 3.04 and 3.15 (s,

3H), 3.50 (t, $J=7.0$, 1H), 3.63 (t, $J=6.9$, 1H), 3.67 (s, 2H), 6.96 (t, $J=8.0$, 1H), 7.04 – 7.09 (m, 2H), 7.55 (d, $J=7.8$, 1H), 8.54 and 8.59 (s, 1H). ^{13}C NMR (101 MHz, CDCl_3) δ = 15.95, 16.06, 26.21, 26.51, 26.74, 28.55, 34.84, 35.04, 35.83, 37.63, 42.32, 48.39, 48.76, 52.86, 55.79, 69.01, 69.42, 83.65, 83.73, 113.71, 113.93, 113.99, 116.78, 119.41, 124.00, 124.07, 128.85, 128.90, 131.01, 131.07, 136.95, 154.32, 154.36.

3-(((2-Cycloheptylethyl)(methyl)amino)methyl)-1H-indol-7-yl methyl(undec-10-yn-1-yl)carbamate (17)

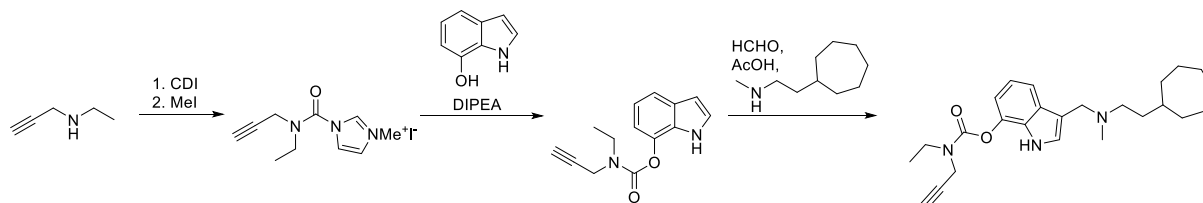
N-Methylundec-10-ynamide was prepared following *GPI* from undec-10-ynoic acid⁸⁷ (2000 mg, 10.97 mmol) and methylamine (2 M in THF), the solvent was removed *in vacuo*, residue partitioned between DCM (20 mL) and 10% citric acid (10 mL), the organic phase extracted with 1 M sodium hydroxide (10 mL), dried with sodium sulfate, and the solvent was removed *in vacuo*. The crude amide was dissolved in anhydrous THF (10 mL), lithium aluminum hydride solution (9.1 mL, 2.0 eq., 2.4 M in THF) was added slowly with stirring under Ar. The reaction mixture was stirred at 50 °C for 12 h and then while being cooled on an icebath, cautiously quenched with brine. The resulting grey solids were suspended in Et₂O (50 mL), sonicated in an ultrasonic cleaning bath for 5 minutes, filtered, and washed with Et₂O (2 × 20 mL). The ethereal extracts were dried over sodium sulfate, filtered, and volatile components evaporated *in vacuo* to afford *N*-methylundec-10-yn-1-amine⁸⁸.

To the crude *N*-methylundec-10-yn-1-amine (1432 mg) in DCM (20 mL) was added CDI (1.2 eq., 1536 mg), stirred for 6 h at rt, the reaction mixture was then extracted with water (40 mL), the organic phase separated, dried with sodium sulfate, and the solvent removed *in vacuo* to afford *N*-methyl-*N*-(undec-10-yn-1-yl)-1*H*-imidazole-1-carboxamide. Yield: 1840 mg (6.68 mmol, 60.9% over three steps) of white waxy semisolid.

3-Methyl-1-(methyl(undec-10-yn-1-yl)carbamoyl)-1*H*-imidazol-3-ium iodide was prepared by stirring *N*-methyl-*N*-(undec-10-yn-1-yl)-1*H*-imidazole-1-carboxamide (1000 mg, 3.63 mmol) and methyl iodide (1.5 eq., 339 μL) in MeCN (5 mL) under Ar for 24 h. The solvent was removed *in vacuo*, the residue dissolved in MeCN (5 mL), 1*H*-indol-7-ol (293 mg, 2.2 mmol) and DIPEA (500 μL) were added, and the reaction mixture stirred at 60 °C for 6 h. The solvent was removed *in vacuo* and 1*H*-indol-7-yl methyl(undec-10-yn-1-yl)carbamate isolated by column chromatography on silica (PE/EtOAc = 5:1). Yield: 539 mg (1.583 mmol, 72.0%) of colourless oil, that was immediately used further.

3-(((2-Cycloheptylethyl)(methyl)amino)methyl)-1*H*-indol-7-yl methyl(undec-10-yn-1-yl)carbamate was prepared following *GPI* from 1*H*-indol-7-yl methyl(undec-10-yn-1-yl)carbamate (300 mg, 0.881 mmol). Yield: 256 mg (0.504 mmol, 57.2%) of beige semisolid. ESI-HRMS: $m/z = 508.3892$ (MH^+); $C_{32}H_{50}N_3O_2$ requires: $m/z = 508.3898$ (MH^+). ν_{max} 3309, 2922, 2853, 2786, 1705, 1460, 1400, 1350, 1306, 1223, 1169, 1123, 1093, 786, 756, 731, 628 cm^{-1} . Purity: UPLC (254 nm): $t_r = 5.333$ min, 99.8% total area. 1H NMR (400 MHz, $CDCl_3$) $\delta = 1.14 - 1.72$ (m, 29H), 1.96 (t, $J=2.4$, 1H), 2.15 – 2.23 (m, 5H), 2.41 – 2.45 (m, 2H), 3.01 and 3.10 (2 x s, 3H), 3.36 (t, $J=7.4$, 1H), 3.46 (t, $J=7.2$, 1H), 3.67 (s, 2H), 6.90 – 6.97 (m, 1H), 7.01 (d, $J=1.9$, 1H), 7.06 (t, $J=7.8$, 1H), 7.55 (dd, $J=3.2$, 7.8, 1H), 8.62 and 8.68 (2 x s, 1H). ^{13}C NMR (101 MHz, $CDCl_3$) $\delta = 18.32$, 26.41, 26.62, 26.66, 27.33, 28.04, 28.37, 28.39, 28.45, 28.62, 28.96, 29.24, 29.37, 34.56, 34.60, 34.75, 34.84, 35.69, 37.54, 42.15, 49.46, 52.74, 55.65, 68.18, 84.60, 113.57, 113.65, 116.50, 116.62, 119.26, 124.12, 128.79, 128.90, 130.99, 136.97, 154.17, 154.32. Two conformers in a 53:47 ratio.

3-(((2-Cycloheptylethyl)(methyl)amino)methyl)-1*H*-indol-7-yl ethyl(prop-2-yn-1-yl)carbamate (18)



N-Ethylprop-2-yn-1-amine⁸⁹ (208 mg, 2.50 mmol) and CDI (1.0 eq., 405 mg) in DCM (5 mL) were stirred at rt for 12 h. The reaction mixture was extracted with water (10 mL, discarded), dried with sodium sulfate, the solvent was removed *in vacuo*, the residue dissolved in MeCN (5 mL), iodomethane (1.2 eq., 187 μ L) was added, and the mixture stirred under Ar at rt for 18 h. The solvent was removed *in vacuo*, the residue redissolved in MeCN (5 mL), 1*H*-indol-7-ol (141 mg, 1.06 mmol) and DIPEA (500 μ L) were added, and the reaction mixture stirred at 60 $^{\circ}C$ for 4 h. The solvent was removed *in vacuo* and 1*H*-indol-7-yl ethyl(prop-2-yn-1-yl)carbamate isolated by column chromatography on silica (PE/EtOAc = 4:1). Yield: 108 mg (0.446 mmol, 42.1%) of brownish oil, which was immediately used further in the next step.

3-(((2-Cycloheptylethyl)(methyl)amino)methyl)-1*H*-indol-7-yl ethyl(prop-2-yn-1-yl)carbamate was prepared following *GPI* from 1*H*-indol-7-yl ethyl(prop-2-yn-1-yl)carbamate (73 mg, 0.301 mmol). Yield: 64 mg (0.156 mmol, 51.9%) of beige oil. ESI-HRMS: $m/z = 410.2797$ (MH^+); $C_{25}H_{36}N_3O_2$ requires: $m/z = 410.2802$ (MH^+).

3-(((2-Cycloheptylethyl)(methyl)amino)methyl)-1*H*-indol-7-yl di(prop-2-yn-1-yl)carbamate (19)

Di(prop-2-yn-1-yl)amine (372 mg, 4.0 mmol) and CDI (1.0 eq., 649 mg) in DCM (5 mL) were stirred at rt for 12 h. The reaction mixture was extracted with water (10 mL, discarded), dried with sodium sulfate, the solvent was removed *in vacuo*, the residue dissolved in MeCN (5 mL), iodomethane (1.2 eq., 299 μ L) was added, and the mixture stirred under Ar at rt for 18 h. The solvent was removed *in vacuo*, the residue redissolved in MeCN (5 mL), 1*H*-indol-7-ol (293 mg, 2.2 mmol) and DIPEA (500 μ L) were added, and the reaction mixture stirred at 60 °C for 4h. The solvent was removed *in vacuo* and 1*H*-indol-7-yl di(prop-2-yn-1-yl)carbamate isolated by column chromatography on silica (PE/EtOAc = 4:1). Yield: 363 mg (1.44 mmol, 65.4%) of beige solid. mp 78.1–79.5 °C. ESI-HRMS: m/z = 253.0958 (MH^+); $C_{15}H_{13}N_2O_2$ requires: m/z = 253.0972 (MH^+). ν_{max} 3303, 3286, 2975, 1691, 1458, 1407, 1340, 1211, 1159, 1103, 963, 850, 788, 723, 638 cm^{-1} . 1H NMR (400 MHz, $CDCl_3$) δ = 2.42 and 2.46 (2 x s, 2H), 4.41 and 4.46 (2 x s, 4H), 6.59 (dd, J =2.1, 3.1, 1H), 7.07 – 7.16 (m, 3H), 7.56 (d, J =7.6, 1H), 8.57 (s, 1H). ^{13}C NMR (101 MHz, $CDCl_3$) δ = 36.10, 36.29, 72.87, 73.40, 77.84, 78.68, 103.03, 113.93, 118.34, 119.70, 124.86, 128.20, 130.80, 136.47, 153.20.

3-(((2-Cycloheptylethyl)(methyl)amino)methyl)-1*H*-indol-7-yl di(prop-2-yn-1-yl)carbamate was prepared following *GPI* from 1*H*-indol-7-yl di(prop-2-yn-1-yl)carbamate (150 mg, 0.595 mmol). Yield: 165 mg (0.393 mmol, 66.1%) of beige oil. ESI-HRMS: m/z = 420.2625 (MH^+); $C_{26}H_{34}N_3O_2$ requires: m/z = 420.2646 (MH^+). ν_{max} 3303, 2920, 2851, 2794, 1716, 1443, 1407, 1345, 1216, 1168, 1101, 731 cm^{-1} . Purity: UPLC (220 nm): t_r = 4.593 min, 98.5% total area. 1H NMR (400 MHz, $CDCl_3$) δ = 1.16 – 1.24 (m, 2H), 1.37 – 1.74 (m, 13H), 2.21 (s, 3H), 2.35 – 2.47 (m, 4H), 3.68 (s, 2H), 4.37 and 4.43 (2 x s, 4H), 7.00 – 7.05 (m, 2H), 7.09 (t, J =7.8, 1H), 7.59 (d, J =7.7, 1H), 8.58 (s, 1H). ^{13}C NMR (101 MHz, $CDCl_3$) δ = 26.47, 28.50, 34.80, 35.75, 36.06, 36.23, 37.57, 42.23, 52.79, 55.74, 72.83, 73.34, 77.82, 78.65, 113.95, 113.99, 117.24, 119.36, 124.10, 128.62, 130.97, 136.38, 153.20.

3-(((2-Cycloheptylethyl)(methyl)amino)methyl)-1*H*-indol-7-yl isopropyl(prop-2-yn-1-yl)carbamate (20)

N-Isopropylprop-2-yn-1-amine⁹⁰ (768 mg, 7.90 mmol) and CDI (1.0 eq., 1281 mg) in DCM (8 mL) were stirred at rt for 12 h. The reaction mixture was extracted with water (15 mL, discarded), dried with sodium sulfate, the solvent was removed *in vacuo*, the residue dissolved in MeCN (5 mL), iodomethane (1.2 eq., 590 μ L) was added, and the mixture stirred under Ar

at rt for 18 h. The solvent was removed *in vacuo*, the residue redissolved in MeCN (5 mL), 1*H*-indol-7-ol (181 mg, 1.36 mmol) and DIPEA (500 μ L) were added, and the reaction mixture stirred at 60 °C for 4 h. The solvent was removed *in vacuo* and 1*H*-indol-7-yl isopropyl(prop-2-yn-1-yl)carbamate isolated by column chromatography on silica (PE/EtOAc = 3:1). Yield: 290 mg (1.13 mmol, 83.1%) of brownish oil. ESI-HRMS: m/z = 257.1281 (MH^+); $C_{15}H_{17}N_2O_2$ requires: m/z = 257.1285 (MH^+). ν_{max} 3421, 3297, 2979, 1698, 1441, 1404, 1332, 1233, 1193, 1067, 891, 781, 722 cm^{-1} . Purity: UPLC (254 nm): t_r = 4.493 min, 99.5% total area. 1H NMR (400 MHz, $CDCl_3$) δ = 1.29 – 1.47 (m, 6H), 2.35 and 2.43 (br s, 1H), 4.15 (s, 2H), 4.54 (hept, J =6.6, 1H), 6.59 – 6.63 (m, 1H), 7.03 – 7.21 (m, 3H), 7.54 – 7.58 (m, 1H), 8.62 and 8.74 (s, 1H). ^{13}C NMR (101 MHz, $CDCl_3$) δ = 20.18, 20.86, 31.78, 32.58, 48.34, 49.09, 71.05, 80.58, 81.86, 102.89, 113.55, 114.00, 117.82, 119.60, 124.58, 124.87, 128.48, 130.52, 130.88, 136.73, 153.12, 153.72. Two sets of conformer signals.

3-(((2-Cycloheptylethyl)(methyl)amino)methyl)-1*H*-indol-7-yl isopropyl(prop-2-yn-1-yl)carbamate was prepared following *GPI* from 1*H*-indol-7-yl isopropyl(prop-2-yn-1-yl)carbamate (141 mg, 0.550 mmol). Yield: 120 mg (0.283 mmol, 51.5%) of beige semisolid. ESI-HRMS: m/z = 424.29504 (MH^+); $C_{26}H_{38}N_3O_2$ requires: m/z = 424.2959 (MH^+). ν_{max} 3308, 2919, 2851, 2788, 1705, 1443, 1406, 1334, 1225, 1197, 1168, 11083, 756, 732 cm^{-1} . Purity: UPLC (220 nm): t_r = 4.723 min, 98.0% total area. 1H NMR (400 MHz, $CDCl_3$) δ = 1.14 – 1.73 (m, 21H), 2.22 (s, 3H), 2.38 and 2.51 (2 x s, 1H), 2.40 – 2.45 (m, 2H), 3.68 (s, 2H), 4.14 (d, J =2.4, 2H), 4.50 (hept, J =6.8, 1H), 6.94 – 7.11 (m, 3H), 7.57 (d, J =8.6, 1H), 8.47 and 8.55 (s, 1H). ^{13}C NMR (101 MHz, $CDCl_3$) δ = 20.37, 21.02, 26.52, 31.96, 32.70, 34.86, 35.86, 37.65, 42.33, 48.44, 49.20, 52.88, 55.78, 71.07, 82.01, 114.08, 114.14, 116.88, 119.44, 123.83, 128.95, 130.81, 136.71, 153.20.

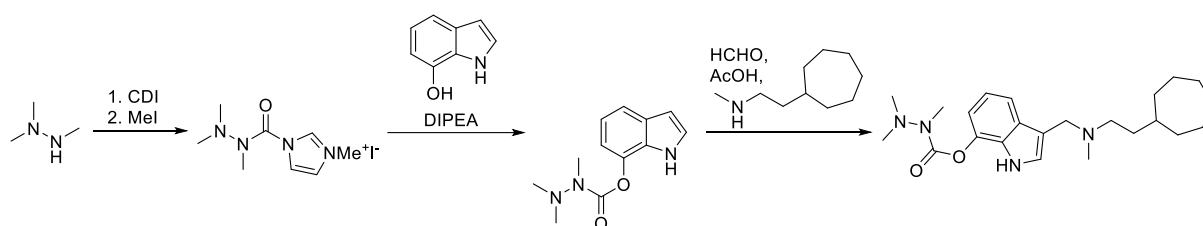
3-(((2-Cycloheptylethyl)(methyl)amino)methyl)-1*H*-indol-7-yl methoxy(methyl)carbamate (21)

1-(Methoxy(methyl)carbamoyl)-3-methyl-1*H*-imidazol-3-ium iodide⁵⁸ (3.0 eq., 713 mg), 1*H*-indol-7-ol (106 mg, 0.8 mmol), and DIPEA (500 μ L) in MeCN (5 mL) were stirred at 60 °C for 4 h. The solvent was removed *in vacuo* and 1*H*-indol-7-yl methoxy(methyl)carbamate isolated by column chromatography on silica (1. PE/EtOAc = 3:1; 2. PE/EtOAc = 1:1). Yield: 156 mg (0.708 mmol, 88.5%) of beige semisolid. ESI-HRMS: m/z = 221.0916 (MH^+); $C_{11}H_{13}N_2O_3$ requires: m/z = 221.0921 (MH^+). ν_{max} 3308, 2940, 1705, 1580, 1458, 1418, 1369, 1341, 1234, 1215, 1164, 1140, 1110, 1042, 1015, 939, 784, 732 cm^{-1} . 1H NMR (400 MHz, $CDCl_3$) δ = 3.32 (s, 3H), 3.81 (s, 3H), 6.56 (dd, J =2.1, 3.1, 1H), 7.04 – 7.14 (m, 3H), 7.53 – 7.56 (m, 1H), 8.85

(s, 1H). ^{13}C NMR (101 MHz, CDCl_3) δ = 35.60, 61.69, 102.79, 113.62, 118.25, 119.55, 125.05, 128.21, 130.93, 136.45, 154.71.

3-(((2-Cycloheptylethyl)(methyl)amino)methyl)-1*H*-indol-7-yl methoxy(methyl)carbamate was prepared following *GPI* from 1*H*-indol-7-yl methoxy(methyl)carbamate (108 mg, 0.490 mmol). Yield: 120 mg (0.310 mmol, 63.3%) of yellowish oil. ESI-HRMS: m/z = 388.2583 (MH^+); $\text{C}_{22}\text{H}_{34}\text{N}_3\text{O}_3$ requires: m/z = 388.2595 (MH^+). ν_{max} 3327, 2919, 2851, 2790, 1724, 1579, 1445, 1346, 1224, 1169, 1045, 980, 731 cm^{-1} . Purity: UPLC (220 nm): t_r = 4.460 min, 99.2% total area. ^1H NMR (400 MHz, CDCl_3) δ = 1.14 – 1.24 (m, 2H), 1.35 – 1.73 (m, 13H), 2.21 (s, 3H), 2.40 – 2.45 (m, 2H), 3.30 (s, 3H), 3.67 (s, 2H), 3.81 (s, 3H), 7.00 (dd, J =0.6, 7.7, 1H), 7.04 (d, J =2.1, 1H), 7.08 (t, J =7.8, 1H), 7.58 (d, J =7.7, 1H), 8.76 (s, 1H). ^{13}C NMR (101 MHz, CDCl_3) δ = 26.49, 28.52, 34.82, 35.74, 37.63, 42.24, 52.74, 55.77, 61.84, 113.72, 113.80, 117.16, 119.34, 124.34, 128.61, 131.13, 136.40, 154.80.

3-(((2-Cycloheptylethyl)(methyl)amino)methyl)-1*H*-indol-7-yl 1,2,2-trimethylhydrazine-1-carboxylate (**22**)



1,1,2-Trimethylhydrazine⁹¹ (3.76 mmol) and CDI (1.0 eq., 610 mg) in DCM (10 mL) were stirred at rt for 12 h. The reaction mixture was extracted with water (10 mL, discarded), dried with sodium sulfate, the solvent was removed *in vacuo*, the residue dissolved in MeCN (5 mL), iodomethane (1.1 eq., 257 μL) was added, and the mixture stirred under Ar at rt for 12 h. Then 1*H*-indol-7-ol (200 mg, 1.5 mmol) and DIPEA (500 μL) were added, and the reaction mixture stirred at 60 $^{\circ}\text{C}$ for 4 h. The solvent was removed *in vacuo* and 1*H*-indol-7-yl 1,2,2-trimethylhydrazine-1-carboxylate isolated by column chromatography on silica (1. PE/EtOAc = 3:1; 2. PE/EtOAc = 1:1). Yield: 211 mg (0.905 mmol, 60.3%) of brownish semisolid. ^1H NMR (400 MHz, CDCl_3) δ = 2.66 (s, 6H), 3.02 and 3.13 (2 x br s, 3H), 6.52 (dd, J =2.1, 3.1, 1H), 6.98 (d, J =7.6, 1H), 7.05 (t, J =7.7, 1H), 7.11 (t, J =2.8, 1H), 7.47 (d, J =7.8, 1H), 8.98 (s, 1H).

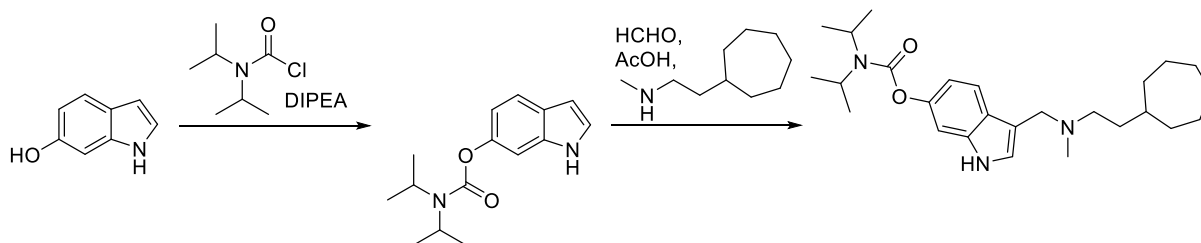
3-(((2-Cycloheptylethyl)(methyl)amino)methyl)-1*H*-indol-7-yl 1,2,2-trimethylhydrazine-1-carboxylate was prepared following *GPI* from 1*H*-indol-7-yl 1,2,2-trimethylhydrazine-1-carboxylate (211 mg, 0.905 mmol). Yield: 184 mg (0.459 mmol, 50.8%) of brownish semisolid.

ESI-HRMS: $m/z = 401.2902$ (MH^+); $C_{23}H_{37}N_4O_2$ requires: $m/z = 401.2911$ (MH^+). ν_{max} 3170, 2920, 2851, 2783, 1718, 1579, 1445, 1347, 1227, 1121, 1021, 908, 730 cm^{-1} . Purity: UPLC (254 nm): $t_r = 4.450$ min, 99.4% total area. 1H NMR (400 MHz, $CDCl_3$) $\delta = 1.11 - 1.22$ (m, 2H), 1.34 – 1.72 (m, 13H), 2.18 (s, 3H), 2.38 – 2.43 (m, 2H), 2.66 (s, 6H), 2.96 – 3.25 (m, 3H), 3.65 (s, 2H), 6.96 (d, $J=7.1$, 1H), 7.02 – 7.07 (m, 2H), 7.52 (dd, $J=0.8$, 7.8, 1H), 8.82 (s, 1H). ^{13}C NMR (101 MHz, $CDCl_3$) $\delta = 26.41, 27.82, 28.45, 31.91, 34.73, 35.62, 37.58, 42.14, 42.44, 43.02, 52.63, 55.67, 113.48, 113.73, 116.63, 119.22, 124.26, 128.79, 130.98, 136.81, 154.72$.

3-(((2-Cycloheptylethyl)(methyl)amino)methyl)-1H-indol-6-yl dimethylcarbamate (23)

1H-Indol-6-ol (prepared from 6-benzyloxyindole as described under **6**, 149 mg, 1.12 mmol), *N,N*-dimethylcarbamoyl chloride (1.1 eq., 103 μ L), and DIPEA (500 μ L) in MeCN (3 mL) were stirred at rt under Ar for 18 h. 1H-Indol-6-yl dimethylcarbamate was isolated by column chromatography on silica (PE/EtOAc = 3:1). Yield: 196 mg (0.960 mmol, 85.7%) of beige semisolid, which was immediately used further following *GPI* to afford 3-(((2-cycloheptylethyl)(methyl)amino)methyl)-1H-indol-6-yl dimethylcarbamate. Yield: 199 mg (0.536 mmol, 55.8%) of beige semisolid. ESI-HRMS: $m/z = 372.2636$ (MH^+); $C_{22}H_{34}N_3O_2$ requires: $m/z = 372.2646$ (MH^+). ν_{max} 3310, 2918, 2851, 2788, 1697, 1626, 1456, 1393, 1343, 1186, 945, 874, 840 cm^{-1} . Purity: UPLC (254 nm): $t_r = 4.403$ min, 96.4% total area. 1H NMR (400 MHz, $CDCl_3$) $\delta = 1.14 - 1.23$ (m, 2H), 1.35 – 1.74 (m, 12H), 2.18 (s, 3H), 2.40 – 2.45 (m, 2H), 3.04 (s, 3H), 3.12 (s, 3H), 3.62 (s, 2H), 6.80 (d, $J=1.4$, 1H), 6.83 (dd, $J=2.1, 8.5$, 2H), 6.98 (d, $J=2.0$, 1H), 7.57 (d, $J=8.5$, 1H), 9.28 (s, 1H). ^{13}C NMR (101 MHz, $CDCl_3$) $\delta = 26.45, 28.50, 34.79, 35.65, 36.46, 36.72, 37.68, 42.06, 52.50, 55.72, 104.59, 111.95, 113.55, 119.24, 124.75, 125.76, 136.12, 146.81, 156.05$.

3-(((2-Cycloheptylethyl)(methyl)amino)methyl)-1H-indol-6-yl diisopropylcarbamate (24)



1H-Indol-6-ol (122 mg, 0.916 mmol), *N,N*-diisopropylcarbamoyl chloride (1.5 eq., 225 mg), and DIPEA (500 μ L) in MeCN (3 mL) were stirred at rt under Ar for 18 h. 1H-Indol-6-yl diisopropylcarbamate was isolated by column chromatography on silica (PE/EtOAc = 4:1). Yield: 70 mg (0.269 mmol, 29.4%) of white solid. ESI-HRMS: $m/z = 261.1594$ (MH^+); $C_{15}H_{21}N_2O_2$ requires: $m/z = 261.1598$ (MH^+). ν_{max} 3365, 2992, 2971, 1696, 1457, 1284, 1137,

1087, 1020, 894, 866, 782, 722 cm^{-1} . Purity: UPLC (220 nm): t_r = 4.703 min, 99.3% total area. ^1H NMR (400 MHz, DMSO) δ = 1.20 – 1.33 (m, 12H), 3.96 – 4.05 (m, 2H), 6.41 (ddd, J =0.9, 1.9, 3.0, 1H), 6.71 (dd, J =2.1, 8.5, 1H), 7.07 – 7.09 (m, 1H), 7.32 – 7.34 (m, 1H), 7.47 (d, J =8.5, 1H), 11.03 (s, 1H). ^{13}C NMR (101 MHz, DMSO) δ = 20.21, 21.18, 45.89, 100.96, 104.34, 113.75, 119.89, 124.94, 125.69, 135.69, 146.23, 153.56.

3-(((2-Cycloheptylethyl)(methyl)amino)methyl)-1*H*-indol-6-yl diisopropylcarbamate was prepared following *GPI* from 1*H*-indol-6-yl diisopropylcarbamate (50 mg, 0.192 mmol). Yield: 59 mg (0.138 mmol, 71.9%) of beige semisolid. ESI-HRMS: m/z = 428.3265 (MH^+); $\text{C}_{26}\text{H}_{42}\text{N}_3\text{O}_2$ requires: m/z = 428.3272 (MH^+). ν_{max} 3290, 2969, 2920, 2852, 2761, 1684, 1431, 1369, 1331, 1301, 1228, 1210, 1146, 1042, 994, 868, 784, 760, 729 cm^{-1} . Purity: UPLC (220 nm): t_r = 4.850 min, 99.0% total area. ^1H NMR (400 MHz, CDCl_3) δ = 1.13 – 1.72 (m, 27H), 2.18 (s, 3H), 2.38 – 2.44 (m, 2H), 3.63 (s, 2H), 3.98 (br s, 1H), 4.17 (br s, 1H), 6.85 (dd, J =2.1, 8.5, 1H), 6.89 (d, J =2.2, 1H), 7.06 (d, J =1.9, 1H), 7.60 (d, J =8.5, 1H), 8.77 (s, 1H). ^{13}C NMR (101 MHz, CDCl_3) δ = 20.64, 21.62, 26.56, 28.62, 34.90, 35.87, 37.71, 42.25, 45.99, 46.96, 52.79, 55.83, 104.60, 112.75, 113.92, 119.57, 124.34, 125.75, 136.31, 146.96, 154.97.

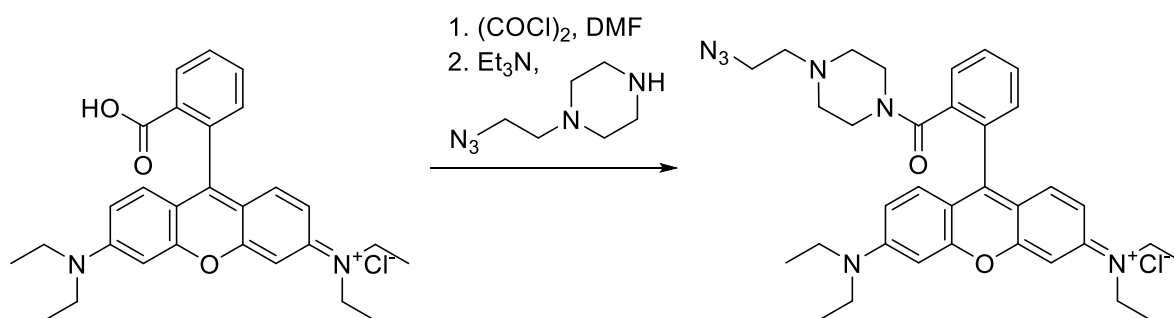
3-(((2-Cycloheptylethyl)(methyl)amino)methyl)-1*H*-indol-6-yl methyl(prop-2-yn-1-yl)carbamate (25)

N-Methylpropargylamine (200 μL , 2.37 mmol) and CDI (1.0 eq., 384 mg) in DCM (5 mL) were stirred at rt for 12 h. The reaction mixture was extracted with water (10 mL, discarded), dried with sodium sulfate, the solvent was removed *in vacuo*, the residue dissolved in MeCN (5 mL), iodomethane (1.5 eq., 221 μL) was added, and the mixture stirred under Ar at rt for 18 h. The solvent was removed *in vacuo*, the residue redissolved in MeCN (5 mL), 1*H*-indol-6-ol (146 mg, 1.1 mmol) and DIPEA (500 μL) were added, and the reaction mixture stirred at 60 $^\circ\text{C}$ for 4 h. The solvent was removed *in vacuo* and 1*H*-indol-6-yl methyl(prop-2-yn-1-yl)carbamate isolated by column chromatography on silica (PE/EtOAc = 3:1). Yield: 200 mg (0.876 mmol, 79.7%) of white solid. mp 145.5–146.1 $^\circ\text{C}$. ESI-HRMS: m/z = 229.0968 (MH^+); $\text{C}_{13}\text{H}_{13}\text{N}_2\text{O}_2$ requires: m/z = 229.0972 (MH^+). ν_{max} 3360, 3293, 3076, 1698, 1453, 1394, 1342, 1286, 1237, 1215, 1152, 1089, 797, 725, 651 cm^{-1} . Purity: UPLC (254 nm): t_r = 4.030 min, 96.9% total area. ^1H NMR (400 MHz, CDCl_3) δ = 2.34 and 2.36 (2 x s, 1H), 3.12 and 3.22 (2 x s, 3H), 4.26 and 4.30 (2 x s, 2H), 6.40 – 6.43 (m, 1H), 6.85 (d, J =8.5, 1H), 6.97 – 6.99 (m, 1H), 7.07 (s, 1H), 7.53 (d, J =8.5, 1H), 8.54 (s, 1H).

3-(((2-Cycloheptylethyl)(methyl)amino)methyl)-1*H*-indol-6-yl methyl(prop-2-yn-1-yl)carbamate was prepared following *GPI* from 1*H*-indol-6-yl methyl(prop-2-yn-1-

yl)carbamate (109 mg, 0.47 mmol). Yield: 20 mg (0.0506 mmol, 10.8%) of beige semisolid. ESI-HRMS: $m/z = 396.2637$ (MH^+); $C_{24}H_{34}N_3O_2$ requires: $m/z = 396.2646$ (MH^+). ν_{max} 3249, 2919, 2850, 2789, 1702, 1456, 1419, 1399, 1343, 1236, 1167, 1125, 1027, 874, 798, 756, 731 cm^{-1} . Purity: UPLC (254 nm): $t_r = 4.470$ min, 98.0% total area. 1H NMR (400 MHz, $CDCl_3$) $\delta = 1.12 - 1.22$ (m, 2H), 1.34 – 1.71 (m, 13H), 2.19 (s, 3H), 2.32 (br s, 1H), 2.39 – 2.44 (m, 2H), 3.10 and 3.20 (2 x s, 3H), 3.64 (s, 2H), 4.25 and 4.29 (2 x s, 2H), 6.85 (dd, $J=1.8, 8.6$, 1H), 6.98 (d, $J=2.2$, 1H), 7.06 (d, $J=1.8$, 1H), 7.61 (d, $J=8.6$, 1H), 8.52 and 8.55 (s, 1H). ^{13}C NMR (101 MHz, $CDCl_3$) $\delta = 26.58, 28.63, 33.87, 34.35, 34.91, 35.85, 37.73, 38.59, 38.81, 42.33, 52.81, 55.89, 72.51, 72.62, 78.67, 104.46, 113.13, 113.88, 119.75, 124.37, 126.00, 136.18, 147.01, 155.12, 155.47$. Two sets of conformer signals.

***N*-(9-(2-(4-(2-Azidoethyl)piperazine-1-carbonyl)phenyl)-6-(diethylamino)-3*H*-xanthen-3-ylidene)-*N*-ethylethanaminium chloride (26)**



N-(9-(2-Carboxyphenyl)-6-(diethylamino)-3*H*-xanthen-3-ylidene)-*N*-ethylethanaminium chloride/Rhodamine B (7000 mg, 14.6 mmol), oxalyl chloride (3.0 eq., 3.71 mL) and DMF (100 μ L) in DCM (50 mL) were stirred under Ar at rt for 3 h (gas efferevescence!), then the volatiles were removed *in vacuo*, the residue was dissolved in toluene (50 mL), the solvent removed *in vacuo*, the residue redissolved in DCM (50 mL), 1-(2-azidoethyl)piperazine⁹² (1.2 eq., 2719 mg) and triethylamine (3.0 eq., 4.07 mL) were added, and the stirring continued at rt for 18 h. The solvent was removed *in vacuo* and the product isolated by column chromatography on silica (1. EtOAc/ $Et_3N = 100:1$; 2. DCM/MeOH = 20:1; 3. DCM/MeOH = 9:1) and *GP2*. Yield: 2657 mg (4.31 mmol, 29.5%) of dark violet semisolid.

Aqueous stability

UPLC analyses were performed as described under Chemistry – General Information. The method used a Waters Acquity UPLC® HSS C18 SB column (2.1 \times 50 mm, 1.8 μ m) thermostated at 40 $^{\circ}C$, with: injection volume, 1 μ L; flow rate, 0.4 mL/min; detector λ , 254 nm;

mobile phase A: 0.1% TFA (v/v) in water; mobile phase B: MeCN. Gradient: 0–5 min, 20–100% B; 5–6 min, 20% B.

Compound stock solutions (10 mM) were prepared in absolute EtOH, while internal standard (caffeine) was dissolved in PBS (0.1 mg/mL). The aqueous stability solutions were prepared by mixing 800 μ L PBS with internal standard, 175 μ L absolute EtOH, and 25 μ L compound stock solution in a HPLC vial to give 250 μ M compound concentration in PBS/EtOH = 80:20, which placed in an autosampler thermostatted at 20 °C, injected immediately and then at hourly intervals for at least 24 hours. The analyte AUCs were normalized on internal standard AUCs and compared with the timepoint zero. For the rate calculation (GraphPad Prism 9.4), pseudo-first order kinetics were presumed (*Table 6*). The stability data show that these carbamates are stable for days in the aqueous solution under physiologically similar conditions.

Table 6: The stability of the investigated compounds in an aqueous solution. * small R^2 values indicate that for a proper rate determination, samples should be observed for much longer time periods. Therefore, the calculated half-lives ($t_{1/2}$) are just rough approximates. #the difference between the last and the first timepoint was smaller than the experimental error (approx. 2%).

| Compound | $t_{1/2}$ | $k [h^{-1}]$ | R^{2*} |
|-----------|---------------------|--------------|----------|
| 8 | ~52 days | 0.000557659 | 0.560 |
| 10 | ~32 days | 0.000900801 | 0.477 |
| 11 | ~26 days | 0.001122123 | 0.505 |
| 18 | ~28 days | 0.001014275 | 0.807 |
| 21 | ~21 days | 0.001366556 | 0.836 |
| 23 | ~35 days | 0.000832989 | 0.667 |
| 6 | stable [#] | | |
| 7 | | | |
| 13 | | | |
| 14 | | | |
| 15 | | | |
| 16 | | | |
| 22 | | | |
| 25 | | | |

Acknowledgements

This research was funded by the Slovenian Research Agency (ARRS), Research Core Funding № P1-0208, P1-0012, project NC-0009, and a young researcher grant to A.M. X.B., M.D. and F.N. were supported by the French Ministry of Armed Forces (Direction Générale de l'Armement and Service de Santé des Armées, NBC-5-C-4210). Dr José Dias is acknowledged for providing recombinant hAChE for the *in vitro* assay. Authors would like to thank the ESRF for long-term beamtime access (MX2329 IBS BAG) and Ažman Computing Centre at National Institute of Chemistry for computational resources.

Abbreviations

ACh – acetylcholine

(h)AChE – (human) acetylcholinesterase

(h)BChE – (human) butyrylcholinesterase

ChE(s) – cholinesterase(s)

ChEI(s) – cholinesterase inhibitor(s)

CuAAC – Copper-Catalyzed Azide-Alkyne Cycloaddition

EtOAc – ethyl acetate

EtOH – ethanol

IRC – intrinsic reaction coordinate

MES – 2-(*N*-morpholino)ethanesulfonic acid

MeCN – acetonitrile

MeOH – methanol

PE – petroleum ether

RA – residual activity

RMSD – root-mean-square deviation

SEM – standard error of the mean

References

- (1) Xing, S.; Li, Q.; Xiong, B.; Chen, Y.; Feng, F.; Liu, W.; Sun, H. Structure and Therapeutic Uses of Butyrylcholinesterase: Application in Detoxification, Alzheimer's Disease, and Fat Metabolism. *Med. Res. Rev.* **2021**, *41* (2), 858–901. <https://doi.org/10.1002/med.21745>.

- (2) Lockridge, O. Review of Human Butyrylcholinesterase Structure, Function, Genetic Variants, History of Use in the Clinic, and Potential Therapeutic Uses. *Pharmacol. Ther.* **2015**, *148*, 34–46. <https://doi.org/10.1016/j.pharmthera.2014.11.011>.
- (3) Miles, J. A.; Ross, B. P. Recent Advances in Virtual Screening for Cholinesterase Inhibitors. *ACS Chem. Neurosci.* **2021**, *12* (1), 30–41. <https://doi.org/10.1021/acschemneuro.0c00627>.
- (4) Jing, L.; Wu, G.; Kang, D.; Zhou, Z.; Song, Y.; Liu, X.; Zhan, P. Contemporary Medicinal-Chemistry Strategies for the Discovery of Selective Butyrylcholinesterase Inhibitors. *Drug Discov. Today* **2019**, *24* (2), 629–635. <https://doi.org/10.1016/j.drudis.2018.11.012>.
- (5) Li, Q.; Xiong, B.; Wang, Y.; Lyu, W.; Xing, S.; Chen, Y.; Liao, Q.; He, S.; Feng, F.; Liu, W.; Chen, Y.; Sun, H. A Highly Effective and Stable Butyrylcholinesterase Inhibitor with Multi-Faceted Neuroprotection and Cognition Improvement. *Eur. J. Med. Chem.* **2022**, *239*, 114510. <https://doi.org/10.1016/j.ejmech.2022.114510>.
- (6) Fernández-Bolaños, J. G.; López, Ó. Butyrylcholinesterase Inhibitors as Potential Anti-Alzheimer's Agents: An Updated Patent Review (2018-Present). *Expert Opin. Ther. Pat.* **2022**, *32* (8), 913–932. <https://doi.org/10.1080/13543776.2022.2083956>.
- (7) Moreira, N. C. dos S.; Lima, J. E. B. de F.; Marchiori, M. F.; Carvalho, I.; Sakamoto-Hojo, E. T. Neuroprotective Effects of Cholinesterase Inhibitors: Current Scenario in Therapies for Alzheimer's Disease and Future Perspectives. *J. Alzheimers Dis. Rep.* **2022**, *6* (1), 177–193. <https://doi.org/10.3233/ADR-210061>.
- (8) Sun, H.; Pang, Y.-P.; Lockridge, O.; Brimijoin, S. Re-Engineering Butyrylcholinesterase as a Cocaine Hydrolase. *Mol. Pharmacol.* **2002**, *62* (2), 220–224. <https://doi.org/10.1124/mol.62.2.220>.
- (9) Zhang, T.; Zheng, X.; Kim, K.; Zheng, F.; Zhan, C.-G. Blocking Drug Activation as a Therapeutic Strategy to Attenuate Acute Toxicity and Physiological Effects of Heroin. *Sci. Rep.* **2018**, *8* (1), 16762. <https://doi.org/10.1038/s41598-018-35196-8>.
- (10) Zhang, H.; Wang, Y.; Wang, Y.; Li, X.; Wang, S.; Wang, Z. Recent Advance on Carbamate-Based Cholinesterase Inhibitors as Potential Multifunctional Agents against Alzheimer's Disease. *Eur. J. Med. Chem.* **2022**, *240*, 114606. <https://doi.org/10.1016/j.ejmech.2022.114606>.
- (11) Scheindlin, S. Episodes in the Story of Physostigmine. *Mol. Interv.* **2010**, *10* (1), 4. <https://doi.org/10.1124/mi.10.1.1>.
- (12) Bar-On, P.; Millard, C. B.; Harel, M.; Dvir, H.; Enz, A.; Sussman, J. L.; Silman, I. Kinetic and Structural Studies on the Interaction of Cholinesterases with the Anti-Alzheimer Drug Rivastigmine. *Biochemistry* **2002**, *41* (11), 3555–3564. <https://doi.org/10.1021/bi020016x>.
- (13) Košak, U.; Strašek, N.; Knez, D.; Jukič, M.; Žakelj, S.; Zahirović, A.; Pišlar, A.; Brazzolotto, X.; Nachon, F.; Kos, J.; Gobec, S. N-Alkylpiperidine Carbamates as Potential Anti-Alzheimer's Agents. *Eur. J. Med. Chem.* **2020**, *197*, 112282. <https://doi.org/10.1016/j.ejmech.2020.112282>.
- (14) Awoonor-Williams, E.; Walsh, A. G.; Rowley, C. N. Modeling Covalent-Modifier Drugs. *Biochim. Biophys. Acta BBA - Proteins Proteomics* **2017**, *1865* (11, Part B), 1664–1675. <https://doi.org/10.1016/j.bbapap.2017.05.009>.
- (15) De Cesco, S.; Kurian, J.; Dufresne, C.; Mittermaier, A. K.; Moitessier, N. Covalent Inhibitors Design and Discovery. *Eur. J. Med. Chem.* **2017**, *138*, 96–114. <https://doi.org/10.1016/j.ejmech.2017.06.019>.
- (16) Flanagan, M. E.; Abramite, J. A.; Anderson, D. P.; Aulabaugh, A.; Dahal, U. P.; Gilbert, A. M.; Li, C.; Montgomery, J.; Oppenheimer, S. R.; Ryder, T.; Schuff, B. P.; Uccello, D. P.; Walker, G. S.; Wu, Y.; Brown, M. F.; Chen, J. M.; Hayward, M. M.; Noe, M. C.;

- Obach, R. S.; Philippe, L.; Shanmugasundaram, V.; Shapiro, M. J.; Starr, J.; Stroh, J.; Che, Y. Chemical and Computational Methods for the Characterization of Covalent Reactive Groups for the Prospective Design of Irreversible Inhibitors. *J. Med. Chem.* **2014**, *57* (23), 10072–10079. <https://doi.org/10.1021/jm501412a>.
- (17) Lonsdale, R.; Burgess, J.; Colclough, N.; Davies, N. L.; Lenz, E. M.; Orton, A. L.; Ward, R. A. Expanding the Armory: Predicting and Tuning Covalent Warhead Reactivity. *J. Chem. Inf. Model.* **2017**, *57* (12), 3124–3137. <https://doi.org/10.1021/acs.jcim.7b00553>.
- (18) Ghosh, A. K.; Brindisi, M. Organic Carbamates in Drug Design and Medicinal Chemistry. *J. Med. Chem.* **2015**, *58* (7), 2895–2940. <https://doi.org/10.1021/jm501371s>.
- (19) Luo, Y. L. Mechanism-Based and Computational-Driven Covalent Drug Design. *J. Chem. Inf. Model.* **2021**, *61* (11), 5307–5311. <https://doi.org/10.1021/acs.jcim.1c01278>.
- (20) Thorarensen, A.; Balbo, P.; Banker, M. E.; Czerwinski, R. M.; Kuhn, M.; Maurer, T. S.; Telliez, J.-B.; Vincent, F.; Wittwer, A. J. The Advantages of Describing Covalent Inhibitor in Vitro Potencies by IC₅₀ at a Fixed Time Point. IC₅₀ Determination of Covalent Inhibitors Provides Meaningful Data to Medicinal Chemistry for SAR Optimization. *Bioorg. Med. Chem.* **2021**, *29*, 115865. <https://doi.org/10.1016/j.bmc.2020.115865>.
- (21) Copeland, R. A. Irreversible Enzyme Inactivators. In *Evaluation of Enzyme Inhibitors in Drug Discovery*; John Wiley & Sons, Ltd, 2013; pp 345–382. <https://doi.org/10.1002/9781118540398.ch9>.
- (22) Hoffmann, M.; Stiller, C.; Endres, E.; Scheiner, M.; Gunesch, S.; Sottriffer, C.; Maurice, T.; Decker, M. Highly Selective Butyrylcholinesterase Inhibitors with Tunable Duration of Action by Chemical Modification of Transferable Carbamate Units Exhibit Pronounced Neuroprotective Effect in an Alzheimer's Disease Mouse Model. *J. Med. Chem.* **2019**, *62* (20), 9116–9140. <https://doi.org/10.1021/acs.jmedchem.9b01012>.
- (23) Groner, E.; Ashani, Y.; Schorer-Apelbaum, D.; Sterling, J.; Herzig, Y.; Weinstock, M. The Kinetics of Inhibition of Human Acetylcholinesterase and Butyrylcholinesterase by Two Series of Novel Carbamates. *Mol. Pharmacol.* **2007**, *71* (6), 1610–1617. <https://doi.org/10.1124/mol.107.033928>.
- (24) Stojan, J. Rapid Mechanistic Evaluation and Parameter Estimation of Putative Inhibitors in a Single-Step Progress-Curve Analysis: The Case of Horse Butyrylcholinesterase. *Molecules* **2017**, *22* (8), 1248. <https://doi.org/10.3390/molecules22081248>.
- (25) Bevc, S.; Konc, J.; Stojan, J.; Hodošček, M.; Penca, M.; Praprotnik, M.; Janežič, D. ENZO: A Web Tool for Derivation and Evaluation of Kinetic Models of Enzyme Catalyzed Reactions. *PLOS ONE* **2011**, *6* (7), e22265. <https://doi.org/10.1371/journal.pone.0022265>.
- (26) Yu, Q.; Holloway, H. W.; Utsuki, T.; Brossi, A.; Greig, N. H. Synthesis of Novel Phenserine-Based-Selective Inhibitors of Butyrylcholinesterase for Alzheimer's Disease. *J. Med. Chem.* **1999**, *42* (10), 1855–1861. <https://doi.org/10.1021/jm980459s>.
- (27) Perola, E.; Cellai, L.; Lamba, D.; Filocamo, L.; Brufani, M. Long Chain Analogs of Physostigmine as Potential Drugs for Alzheimer's Disease: New Insights into the Mechanism of Action in the Inhibition of Acetylcholinesterase. *Biochim. Biophys. Acta BBA - Protein Struct. Mol. Enzymol.* **1997**, *1343* (1), 41–50. [https://doi.org/10.1016/S0167-4838\(97\)00133-7](https://doi.org/10.1016/S0167-4838(97)00133-7).
- (28) Sawatzky, E.; Wehle, S.; Kling, B.; Wendrich, J.; Bringmann, G.; Sottriffer, C. A.; Heilmann, J.; Decker, M. Discovery of Highly Selective and Nanomolar Carbamate-Based Butyrylcholinesterase Inhibitors by Rational Investigation into Their Inhibition Mode. *J. Med. Chem.* **2016**, *59* (5), 2067–2082. <https://doi.org/10.1021/acs.jmedchem.5b01674>.

- (29) Scheiner, M.; Sink, A.; Hoffmann, M.; Vrigneau, C.; Endres, E.; Carles, A.; Sottriffer, C.; Maurice, T.; Decker, M. Photoswitchable Pseudoirreversible Butyrylcholinesterase Inhibitors Allow Optical Control of Inhibition in Vitro and Enable Restoration of Cognition in an Alzheimer's Disease Mouse Model upon Irradiation. *J. Am. Chem. Soc.* **2022**, *144* (7), 3279–3284. <https://doi.org/10.1021/jacs.1c13492>.
- (30) Venkatasubban, K. S.; Johnson, J. L.; Thomas, J. L.; Fauq, A.; Cusack, B.; Rosenberry, T. L. Decarbamylation of Acetylcholinesterases Is Markedly Slowed as Carbamoyl Groups Increase in Size. *Arch. Biochem. Biophys.* **2018**, *655*, 67–74. <https://doi.org/10.1016/j.abb.2018.08.006>.
- (31) Ballard, C. G.; Greig, N. H.; Guillozet-Bongaarts, A. L.; Enz, A.; Darvesh, S. Cholinesterases: Roles in the Brain During Health and Disease. *Curr. Alzheimer Res.* **2** (3), 307–318.
- (32) Gabriel, A. J.; Almeida, M. R.; Ribeiro, M. H.; Durães, J.; Tábuas-Pereira, M.; Pinheiro, A. C.; Pascoal, R.; Santana, I.; Baldeiras, I. Association between Butyrylcholinesterase and Cerebrospinal Fluid Biomarkers in Alzheimer's Disease Patients. *Neurosci. Lett.* **2017**, *641*, 101–106. <https://doi.org/10.1016/j.neulet.2017.01.036>.
- (33) Moore, S. W.; Johnson, G. Acetylcholinesterase in Hirschsprung's Disease. *Pediatr. Surg. Int.* **2005**, *21* (4), 255–263. <https://doi.org/10.1007/s00383-005-1383-z>.
- (34) Agrawal, R. K.; Kakkar, N.; Vasishta, R. K.; Kumari, V.; Samujh, R.; Rao, K. L. N. Acetylcholinesterase Histochemistry (AChE) - A Helpful Technique in the Diagnosis and in Aiding the Operative Procedures of Hirschsprung Disease. *Diagn. Pathol.* **2015**, *10* (1), 208. <https://doi.org/10.1186/s13000-015-0443-5>.
- (35) Thorne, M. W. D.; Cash, M. K.; Reid, G. A.; Burley, D. E.; Luke, D.; Pottie, I. R.; Darvesh, S. Imaging Butyrylcholinesterase in Multiple Sclerosis. *Mol. Imaging Biol.* **2021**, *23* (1), 127–138. <https://doi.org/10.1007/s11307-020-01540-6>.
- (36) Darvesh, S.; LeBlanc, A. M.; Macdonald, I. R.; Reid, G. A.; Bhan, V.; Macaulay, R. J.; Fisk, J. D. Butyrylcholinesterase Activity in Multiple Sclerosis Neuropathology. *Chem. Biol. Interact.* **2010**, *187* (1), 425–431. <https://doi.org/10.1016/j.cbi.2010.01.037>.
- (37) Chao, S.; Krejci, E.; Bernard, V.; Leroy, J.; Jean, L.; Renard, P.-Y. A Selective and Sensitive Near-Infrared Fluorescent Probe for Acetylcholinesterase Imaging. *Chem. Commun.* **2016**, *52* (77), 11599–11602. <https://doi.org/10.1039/C6CC05936H>.
- (38) Ma, Y.; Gao, W.; Ma, S.; Liu, Y.; Lin, W. Observation of the Elevation of Cholinesterase Activity in Brain Glioma by a Near-Infrared Emission Chemosensor. *Anal. Chem.* **2020**, *92* (19), 13405–13410. <https://doi.org/10.1021/acs.analchem.0c02770>.
- (39) Wu, X.; An, J. M.; Shang, J.; Huh, E.; Qi, S.; Lee, E.; Li, H.; Kim, G.; Ma, H.; Oh, M. S.; Kim, D.; Yoon, J. A Molecular Approach to Rationally Constructing Specific Fluorogenic Substrates for the Detection of Acetylcholinesterase Activity in Live Cells, Mice Brains and Tissues. *Chem. Sci.* **2020**, *11* (41), 11285–11292. <https://doi.org/10.1039/D0SC04213G>.
- (40) Xiang, C.; Dirak, M.; Luo, Y.; Peng, Y.; Cai, L.; Gong, P.; Zhang, P.; Kolemen, S. A Responsive AIE-Active Fluorescent Probe for Visualization of Acetylcholinesterase Activity in Vitro and in Vivo. *Mater. Chem. Front.* **2022**, *6* (11), 1515–1521. <https://doi.org/10.1039/D2QM00239F>.
- (41) Fortibui, M. M.; Jang, M.; Lee, S.; Ryoo, I.-J.; Ahn, J. S.; Ko, S.-K.; Kim, J. Near-Infrared Fluorescence Probe for Specific Detection of Acetylcholinesterase and Imaging in Live Cells and Zebrafish. *ACS Appl. Bio Mater.* **2022**, *5* (5), 2232–2239. <https://doi.org/10.1021/acsabm.2c00084>.
- (42) Wang, X.; Li, P.; Ding, Q.; Wu, C.; Zhang, W.; Tang, B. Observation of Acetylcholinesterase in Stress-Induced Depression Phenotypes by Two-Photon

- Fluorescence Imaging in the Mouse Brain. *J. Am. Chem. Soc.* **2019**, *141* (5), 2061–2068. <https://doi.org/10.1021/jacs.8b11414>.
- (43) Yang, Y.; Zhang, L.; Wang, J.; Cao, Y.; Qin, W.; Liu, Y. Real-Time Fluorescent Determination and Biological Imaging in Living Models via a Butyrylcholinesterase-Activated Fluorescent Probe. *Dyes Pigments* **2022**, 110596. <https://doi.org/10.1016/j.dyepig.2022.110596>.
 - (44) Xiang, C.; Xiang, J.; Yang, X.; Li, C.; Zhou, L.; Jiang, D.; Peng, Y.; Xu, Z.; Deng, G.; Zhu, B.; Zhang, P.; Cai, L.; Gong, P. Ratiometric Imaging of Butyrylcholinesterase Activity in Mice with Nonalcoholic Fatty Liver Using an AIE-Based Fluorescent Probe. *J. Mater. Chem. B* **2022**, *10* (22), 4254–4260. <https://doi.org/10.1039/D2TB00422D>.
 - (45) Zhang, Q.; Fu, C.; Guo, X.; Gao, J.; Zhang, P.; Ding, C. Fluorescent Determination of Butyrylcholinesterase Activity and Its Application in Biological Imaging and Pesticide Residue Detection. *ACS Sens.* **2021**, *6* (3), 1138–1146. <https://doi.org/10.1021/acssensors.0c02398>.
 - (46) Wang, L.; Du, C.; Liu, H.; Qiu, W.; Lu, X.; Hu, Y.; Li, Y.; Sun, T.; Chen, Y.; Sun, H. A Practical and High-Affinity Fluorescent Probe for Butyrylcholinesterase: A Good Strategy for Binding Affinity Characterization. *Chin. J. Chem.* **2022**, *40* (11), 1285–1292. <https://doi.org/10.1002/cjoc.202100910>.
 - (47) Liu, S.-Y.; Xiong, H.; Yang, J.-Q.; Yang, S.-H.; Li, Y.; Yang, W.-C.; Yang, G.-F. Discovery of Butyrylcholinesterase-Activated Near-Infrared Fluorogenic Probe for Live-Cell and In Vivo Imaging. *ACS Sens.* **2018**, *3* (10), 2118–2128. <https://doi.org/10.1021/acssensors.8b00697>.
 - (48) Koelle, G. B.; Friedenwald, J. S. A Histochemical Method for Localizing Cholinesterase Activity. *Proc. Soc. Exp. Biol. Med.* **1949**, *70* (4), 617–622. <https://doi.org/10.3181/00379727-70-17013>.
 - (49) Renard, P.-Y.; Jean, L. Probing the Cholinergic System to Understand Neurodegenerative Diseases. *Future Med. Chem.* **2017**, *9* (2), 131–133. <https://doi.org/10.4155/fmc-2016-0213>.
 - (50) Yu, Q.; Liao, J.; Xu, F.; Yuan, X.; Xiong, X.; Xiao, T.; Yu, H.; Huang, K. Developments of Spectroscopic Biosensors for Cholinesterase and Its Inhibitors in the Last Decade: An Overview. *Appl. Spectrosc. Rev.* **2021**, *0* (0), 1–25. <https://doi.org/10.1080/05704928.2021.1990080>.
 - (51) Rajapaksha, A. A.; Fu, Y.-X.; Guo, W. Y.; Liu, S.-Y.; Li, Z.-W.; Xiong, C.-Q.; Yang, W.-C.; Yang, G.-F. Review on the Recent Progress in the Development of Fluorescent Probes Targeting Enzymes. *Methods Appl. Fluoresc.* **2021**, *9* (3), 032001. <https://doi.org/10.1088/2050-6120/abf988>.
 - (52) Speers, A. E.; Cravatt, B. F. Profiling Enzyme Activities In Vivo Using Click Chemistry Methods. *Chem. Biol.* **2004**, *11* (4), 535–546. <https://doi.org/10.1016/j.chembiol.2004.03.012>.
 - (53) Parker, C. G.; Pratt, M. R. Click Chemistry in Proteomic Investigations. *Cell* **2020**, *180* (4), 605–632. <https://doi.org/10.1016/j.cell.2020.01.025>.
 - (54) Bourne, Y.; Kolb, H. C.; Radić, Z.; Sharpless, K. B.; Taylor, P.; Marchot, P. Freeze-Frame Inhibitor Captures Acetylcholinesterase in a Unique Conformation. *Proc. Natl. Acad. Sci.* **2004**, *101* (6), 1449–1454. <https://doi.org/10.1073/pnas.0308206100>.
 - (55) Lewis, W. G.; Green, L. G.; Grynszpan, F.; Radić, Z.; Carlier, P. R.; Taylor, P.; Finn, M. G.; Sharpless, K. B. Click Chemistry In Situ: Acetylcholinesterase as a Reaction Vessel for the Selective Assembly of a Femtomolar Inhibitor from an Array of Building Blocks. *Angew. Chem. Int. Ed.* **2002**, *41* (6), 1053–1057. [https://doi.org/10.1002/1521-3773\(20020315\)41:6<1053::AID-ANIE1053>3.0.CO;2-4](https://doi.org/10.1002/1521-3773(20020315)41:6<1053::AID-ANIE1053>3.0.CO;2-4).

- (56) Manetsch, R.; Krasinski, A.; Radić, Z.; Raushel, J.; Taylor, P.; Sharpless, K. B.; Kolb, H. C. In Situ Click Chemistry: Enzyme Inhibitors Made to Their Own Specifications. *J. Am. Chem. Soc.* **2004**, *126* (40), 12809–12818. <https://doi.org/10.1021/ja046382g>.
- (57) Meden, A.; Knez, D.; Brazzolotto, X.; Nachon, F.; Dias, J.; Svete, J.; Stojan, J.; Grošelj, U.; Gobec, S. From Tryptophan-Based Amides to Tertiary Amines: Optimization of a Butyrylcholinesterase Inhibitor Series. *Eur. J. Med. Chem.* **2022**, *234*, 114248. <https://doi.org/10.1016/j.ejmech.2022.114248>.
- (58) Grzyb, J. A.; Shen, M.; Yoshina-Ishii, C.; Chi, W.; Brown, R. S.; Batey, R. A. Carbamoylimidazolium and Thiocarbamoylimidazolium Salts: Novel Reagents for the Synthesis of Ureas, Thioureas, Carbamates, Thiocarbamates and Amides. *Tetrahedron* **2005**, *61* (30), 7153–7175. <https://doi.org/10.1016/j.tet.2005.05.056>.
- (59) Singh, J.; Petter, R. C.; Baillie, T. A.; Whitty, A. The Resurgence of Covalent Drugs. *Nat. Rev. Drug Discov.* **2011**, *10* (4), 307–317. <https://doi.org/10.1038/nrd3410>.
- (60) Brazzolotto, X.; Igert, A.; Guillon, V.; Santoni, G.; Nachon, F. Bacterial Expression of Human Butyrylcholinesterase as a Tool for Nerve Agent Bioscavengers Development. *Molecules* **2017**, *22* (11), 1828. <https://doi.org/10.3390/molecules22111828>.
- (61) ExPASy - ProtParam tool. <https://web.expasy.org/protparam/> (accessed 2022-07-25).
- (62) Arsov, Z.; Švajger, U.; Mravljak, J.; Pajk, S.; Kotar, A.; Urbančič, I.; Štrancar, J.; Anderluh, M. Internalization and Accumulation in Dendritic Cells of a Small PH-Activatable Glycomimetic Fluorescent Probe as Revealed by Spectral Detection. *ChemBioChem* **2015**, *16* (18), 2660–2667. <https://doi.org/10.1002/cbic.201500376>.
- (63) Dighe, S. N.; De la Mora, E.; Chan, S.; Kantham, S.; McColl, G.; Miles, J. A.; Veliyath, S. K.; Sreenivas, B. Y.; Nassar, Z. D.; Silman, I.; Sussman, J. L.; Weik, M.; McGear, R. P.; Parat, M.-O.; Brazzolotto, X.; Ross, B. P. Rivastigmine and Metabolite Analogues with Putative Alzheimer's Disease-Modifying Properties in a Caenorhabditis Elegans Model. *Commun. Chem.* **2019**, *2* (1), 1–14. <https://doi.org/10.1038/s42004-019-0133-4>.
- (64) Speers, A. E.; Cravatt, B. F. Activity-Based Protein Profiling (ABPP) and Click Chemistry (CC)—ABPP by MudPIT Mass Spectrometry. *Curr. Protoc. Chem. Biol.* **2009**, *1* (1), 29–41. <https://doi.org/10.1002/9780470559277.ch090138>.
- (65) Nachon, F.; Nicolet, Y.; Viguié, N.; Masson, P.; Fontecilla-Camps, J. C.; Lockridge, O. Engineering of a Monomeric and Low-Glycosylated Form of Human Butyrylcholinesterase. *Eur. J. Biochem.* **2002**, *269* (2), 630–637. <https://doi.org/10.1046/j.0014-2956.2001.02692.x>.
- (66) Brazzolotto, X.; Wandhammer, M.; Ronco, C.; Trovaslet, M.; Jean, L.; Lockridge, O.; Renard, P.-Y.; Nachon, F. Human Butyrylcholinesterase Produced in Insect Cells: Huprine-Based Affinity Purification and Crystal Structure. *FEBS J.* **2012**, *279* (16), 2905–2916. <https://doi.org/10.1111/j.1742-4658.2012.08672.x>.
- (67) Kabsch, W. XDS. *Acta Crystallogr. D Biol. Crystallogr.* **2010**, *66* (2), 125–132. <https://doi.org/10.1107/S0907444909047337>.
- (68) Afonine, P. V.; Poon, B. K.; Read, R. J.; Sobolev, O. V.; Terwilliger, T. C.; Urzhumtsev, A.; Adams, P. D. Real-Space Refinement in PHENIX for Cryo-EM and Crystallography. *Acta Crystallogr. Sect. Struct. Biol.* **2018**, *74* (6), 531–544. <https://doi.org/10.1107/S2059798318006551>.
- (69) Moriarty, N. W.; Grosse-Kunstleve, R. W.; Adams, P. D. Electronic Ligand Builder and Optimization Workbench (ELBOW): A Tool for Ligand Coordinate and Restraint Generation. *Acta Crystallogr. Sect. D* **2009**, *65* (10), 1074–1080. <https://doi.org/10.1107/S0907444909029436>.
- (70) Emsley, P.; Lohkamp, B.; Scott, W. G.; Cowtan, K. Features and Development of Ict Coot. *Acta Crystallogr. Sect. D* **2010**, *66* (4), 486–501. <https://doi.org/10.1107/S0907444910007493>.

- (71) Wenig, P.; Odermatt, J. OpenChrom: A Cross-Platform Open Source Software for the Mass Spectrometric Analysis of Chromatographic Data. *BMC Bioinformatics* **2010**, *11* (1), 405. <https://doi.org/10.1186/1471-2105-11-405>.
- (72) Marty, M. T.; Baldwin, A. J.; Marklund, E. G.; Hochberg, G. K. A.; Benesch, J. L. P.; Robinson, C. V. Bayesian Deconvolution of Mass and Ion Mobility Spectra: From Binary Interactions to Polydisperse Ensembles. *Anal. Chem.* **2015**, *87* (8), 4370–4376. <https://doi.org/10.1021/acs.analchem.5b00140>.
- (73) Bowers, K. J.; Chow, E.; Xu, H.; Dror, R. O.; Eastwood, M. P.; Gregersen, B. A.; Klepeis, J. L.; Kolossvary, I.; Moraes, M. A.; Sacerdoti, F. D.; Salmon, J. K.; Shan, Y.; Shaw, D. E. Scalable Algorithms for Molecular Dynamics Simulations on Commodity Clusters. In *Proceedings of the 2006 ACM/IEEE conference on Supercomputing*; SC '06; Association for Computing Machinery: New York, NY, USA, 2006; pp 84-es. <https://doi.org/10.1145/1188455.1188544>.
- (74) Shelley, J. C.; Cholleti, A.; Frye, L. L.; Greenwood, J. R.; Timlin, M. R.; Uchimaya, M. Epik: A Software Program for PKaprediction and Protonation State Generation for Drug-like Molecules. *J. Comput. Aided Mol. Des.* **2007**, *21* (12), 681–691. <https://doi.org/10.1007/s10822-007-9133-z>.
- (75) Olsson, M. H. M.; Søndergaard, C. R.; Rostkowski, M.; Jensen, J. H. PROPKA3: Consistent Treatment of Internal and Surface Residues in Empirical PKa Predictions. *J. Chem. Theory Comput.* **2011**, *7* (2), 525–537. <https://doi.org/10.1021/ct100578z>.
- (76) Jorgensen, W. L.; Maxwell, D. S.; Tirado-Rives, J. Development and Testing of the OPLS All-Atom Force Field on Conformational Energetics and Properties of Organic Liquids. *J. Am. Chem. Soc.* **1996**, *118* (45), 11225–11236. <https://doi.org/10.1021/ja9621760>.
- (77) Banks, J. L.; Beard, H. S.; Cao, Y.; Cho, A. E.; Damm, W.; Farid, R.; Felts, A. K.; Halgren, T. A.; Mainz, D. T.; Maple, J. R.; Murphy, R.; Philipp, D. M.; Repasky, M. P.; Zhang, L. Y.; Berne, B. J.; Friesner, R. A.; Gallicchio, E.; Levy, R. M. Integrated Modeling Program, Applied Chemical Theory (IMPACT). *J. Comput. Chem.* **2005**, *26* (16), 1752–1780. <https://doi.org/10.1002/jcc.20292>.
- (78) Friesner, R. A.; Murphy, R. B.; Repasky, M. P.; Frye, L. L.; Greenwood, J. R.; Halgren, T. A.; Sanschagrin, P. C.; Mainz, D. T. Extra Precision Glide: Docking and Scoring Incorporating a Model of Hydrophobic Enclosure for Protein-Ligand Complexes. *J. Med. Chem.* **2006**, *49* (21), 6177–6196. <https://doi.org/10.1021/jm051256o>.
- (79) Zhu, K.; Borrelli, K. W.; Greenwood, J. R.; Day, T.; Abel, R.; Farid, R. S.; Harder, E. Docking Covalent Inhibitors: A Parameter Free Approach to Pose Prediction and Scoring. *J. Chem. Inf. Model.* **2014**, *54* (7), 1932–1940. <https://doi.org/10.1021/ci500118s>.
- (80) Jorgensen, W. L.; Chandrasekhar, J.; Madura, J. D.; Impey, R. W.; Klein, M. L. Comparison of Simple Potential Functions for Simulating Liquid Water. *J. Chem. Phys.* **1983**, *79* (2), 926–935. <https://doi.org/10.1063/1.445869>.
- (81) Bochevarov, A. D.; Harder, E.; Hughes, T. F.; Greenwood, J. R.; Braden, D. A.; Philipp, D. M.; Rinaldo, D.; Halls, M. D.; Zhang, J.; Friesner, R. A. Jaguar: A High-Performance Quantum Chemistry Software Program with Strengths in Life and Materials Sciences. *Int. J. Quantum Chem.* **2013**, *113* (18), 2110–2142. <https://doi.org/10.1002/qua.24481>.
- (82) Meden, A.; Knez, D.; Jukič, M.; Brazzolotto, X.; Gršič, M.; Pišlar, A.; Zahirović, A.; Kos, J.; Nachon, F.; Svete, J.; Gobec, S.; Grošelj, U. Tryptophan-Derived Butyrylcholinesterase Inhibitors as Promising Leads against Alzheimer's Disease. *Chem. Commun.* **2019**, *55* (26), 3765–3768. <https://doi.org/10.1039/C9CC01330J>.

- (83) Harada, H.; Fujii, A.; Kato, S. An Efficient and Practical Synthesis of N , N -Diethyl-7-Indolyloxyacetamide via 7-Hydroxyindole. *Synth. Commun.* **2003**, *33* (3), 507–514. <https://doi.org/10.1081/SCC-120015783>.
- (84) Pearson, S. E.; Fillery, S. M.; Goldberg, K.; Demeritt, J. E.; Eden, J.; Finlayson, J.; Patel, A. Synthesis of Indole-Dihydroisoquinoline Sulfonyl Ureas via Three-Component Reactions. *Synthesis* **2018**, *50* (24), 4963–4981. <https://doi.org/10.1055/s-0037-1610223>.
- (85) Nudelman, A.; Weinstock-Rosin, M. Indole, Indoline Derivatives, Compositions Comprising Them and Uses Thereof. WO2013150529A2, October 10, 2013.
- (86) Khanna, A.; Maung, C.; Johnson, K. R.; Luong, T. T.; Van Vranken, D. L. Carbenylative Amination with N-Tosylhydrazones. *Org. Lett.* **2012**, *14* (12), 3233–3235. <https://doi.org/10.1021/ol301385g>.
- (87) Narasimhan, S.; Mohan, H.; Palani, N. An Improved Procedure for the Synthesis of Terminal and Internal Alkynes from 10-Undecenoic Acid. *Synth. Commun.* **1991**, *21* (18–19), 1941–1949. <https://doi.org/10.1080/00397919108021786>.
- (88) Epsztein, R.; Le Goff, N. Synthèse de bases de mannich acétyleniques cycliques. *Tetrahedron Lett.* **1985**, *26* (27), 3203–3206. [https://doi.org/10.1016/S0040-4039\(00\)98152-8](https://doi.org/10.1016/S0040-4039(00)98152-8).
- (89) Chukhajian, E. O.; Ayrapetyan, L. V.; Mkrtchyan, H. S.; Panosyan, H. A. Synthesis of Mixed Secondary and Tertiary Amines. *Russ. J. Org. Chem.* **2020**, *56* (2), 353–355. <https://doi.org/10.1134/S1070428020010311>.
- (90) Veguillas, M.; Rosair, G. M.; Bebbington, M. W. P.; Lee, A.-L. Silver Effect in Regiodivergent Gold-Catalyzed Hydroaminations. *ACS Catal.* **2019**, *9* (3), 2552–2557. <https://doi.org/10.1021/acscatal.9b00249>.
- (91) García-Rubio, S.; Wilson, C. D.; Renner, D. A.; Rosser, J. O.; Patra, D.; Reid, J. G.; Pines, S. H. An Improved Process for the Preparation of Trimethylhydrazine and Its Coupling with an Activated Acid Intermediate. *Org. Process Res. Dev.* **2004**, *8* (3), 360–362. <https://doi.org/10.1021/op0342022>.
- (92) Tahtaoui, C.; Parrot, I.; Klotz, P.; Guillier, F.; Galzi, J.-L.; Hibert, M.; Ilien, B. Fluorescent Pirenzepine Derivatives as Potential Bitopic Ligands of the Human M1 Muscarinic Receptor. *J. Med. Chem.* **2004**, *47* (17), 4300–4315. <https://doi.org/10.1021/jm040800a>.